NASA Technical Memorandum 72859

Effect of Number of Probes and Their Orientation on the Calculation of Several Compressor Face Distortion Descriptors

Frederick Stoll, Jeffrey W. Tremback,
and Henry H. Arnaiz

MAY 1979

NASA

NASA Technical Memorandum 72859

Effect of Number of Probes and Their Orientation on the Calculation of Several Compressor Face Distortion Descriptors

Frederick Stoll, Jeffrey W. Tremback,
and Henry H. Arnaiz
Dryden Flight Research Center
Edwards, California

National Aeronautics
and Space Administration

**Scientific and Technical
Information Office**

1979

EFFECT OF NUMBER OF PROBES AND THEIR ORIENTATION ON THE CALCULATION OF SEVERAL COMPRESSOR FACE DISTORTION DESCRIPTORS

Frederick Stoll, Jeffrey W. Tremback, and
Henry H. Arnaiz
Dryden Flight Research Center

INTRODUCTION

Distortion in the flow entering the compressor or fan of a jet engine can affect the performance and stability of that engine considerably. Therefore the accurate measurement of distortion is important during the design, testing, and operation of inlet/engine systems.

The techniques presently being used to measure distortion rely on distortion descriptors that are calculated from various total pressure measurements made in the flow just in front of the engine. The pressure measurements are usually made with radially arranged sets of rakes at the engine compressor face. Each rake contains several probes that are placed along the rakes in such a way as to be located at the centers of equal compressor face areas.

Many different types of descriptors have been and are being used with various degrees of success, as are various rake/probe arrangements. However, typical arrays contain about 40 probes. Most descriptors measure radial, circumferential, or combined radial and circumferential distortion.

Two factors that affect the accuracy of the distortion descriptors are the number of probes and the configuration of the probe array used for the calculation. Many studies, among them reference 1, have attempted to determine the effects of these factors on the calculation of the distortion descriptors. However, either the description of the distortion patterns used in the investigations has been limited, or the number of probes has been insufficient to calculate a representative level of distortion.

During recent tests in the NASA Ames Research Center Unitary Plan Wind Tunnel facility (ref. 2), 320 steady state total pressure measurements were made at the engine compressor face of a mixed-compression inlet. The inlet was a one-third-scale model of the inlet on the Mach 3-plus YF-12 airplane. Three total pressure distortion patterns that were representative of those obtained in flight (refs. 3 and 4) were investigated. The effects of probe number and location on the accuracy of five distortion descriptors were investigated by calculating distortion under steady state conditions with various subsets of the 320-probe array. The number of probes in each subset used to calculate the descriptors ranged from 320 to 20. The effects of probe location were evaluated by comparing distortion values acquired with the same probe configurations in different locations. Total pressure contours constructed from different numbers of probes were also compared, as were values of average compressor face total pressure.

SYMBOLS

A, B	dummy variables in equation for K_θ (table 3)
IDC	circumferential distortion descriptor (table 3)
IDT	combined (maximum-minus-minimum-over-average-pressure) distortion descriptor (table 3)
K	arbitrary distortion descriptor
K_a	combined (K_θ plus K_r) distortion descriptor
K_r	radial distortion descriptor (table 3)
K_θ	circumferential distortion descriptor (table 3)
NP	number of probes per rake
NR	number of rakes
p_{t_0}	free-stream total pressure, N/m^2
p_{t_2}	compressor face total pressure, N/m^2
$\overline{p_{t_2}}$	average p_{t_2}, N/m^2

$\overline{q_2}$ average dynamic pressure at compressor face, N/m^2

R radius

R_{cb} centerbody radius at compressor face (fig. 4)

R_i radius of probe ring i at compressor face, cm

R_o cowl radius at compressor face (fig. 4), cm

θ angular location at compressor face referenced to inlet plane of symmetry (fig. 4), deg

θ_j angular location of rake j, deg

$\Delta\theta_j = \left(\theta_{j+1} - \theta_{j-1}\right)/2$, deg

ε error, percent

Subscripts:

i probe ring

j probe rake

max maximum

min minimum

320 referenced to the 320-probe array

WIND TUNNEL MODEL

The inlet used in this investigation (figs. 1 and 2) was a one-third-scale model of the inlet of the YF-12 airplane (ref. 5). The inlet is of the mixed-compression, axisymmetric type. A slight bend in the centerline causes the inlet to have some nonaxisymmetric characteristics; however, the inlet is symmetric about a vertical lengthwise plane (fig. 2).

The shock waves associated with the operation of the inlet in the mixed-compression mode are shown in figure 3. At supersonic speeds, oblique external and internal shock waves compress the inlet air and reduce its speed to a Mach number slightly above 1.0 at the inlet throat. The inlet air is slowed to subsonic speeds by a normal shock wave at or downstream of the inlet throat.

Several components are used for efficient inlet operation in the mixed-compression mode. To keep the throat Mach number slightly above 1.0 at different flight conditions, the throat area is changed by moving the spike fore and aft. Forward and aft bypass doors are used to keep the normal shock wave just downstream of the inlet throat. Boundary layer bleeds on the spike and the cowl remove boundary layer air from these surfaces in the vicinity of the inlet throat. The removal of boundary layer air just upstream of the terminal shock reduces the shock/boundary layer interaction and allows stable operation in the mixed-compression mode. A fixed mass flow plug was used in conjunction with a sliding cowl to control the corrected engine airflow through the inlet duct.

The engine compressor face is located just downstream of four centerbody support struts and the aft bypass door openings (fig. 2). The struts, which support the spike and centerbody, are airfoil shaped and are located symmetrically with respect to the inlet palne of symmetry (inset, fig. 2). The maximum width of the strut is approximately one-fifth of the compressor face radius.

This inlet was designed and built to simulate the actual flight hardware. It had many components and flow passages, plenums, and exits that were not pertinent to this investigation and are therefore not described herein. However, they are described in references 2, 4, and 5.

MEASUREMENT SYSTEMS

The total pressure measurements at the inlet compressor face were obtained with a special eight-rake/40-probe apparatus. The apparatus consisted of eight fixed, radially arranged rakes with five equal-area-weighted probes per rake. The entire apparatus was capable of being rotated clockwise through any angle up to and including an increment of 45°. The eight-rake configuration is shown with one rake alined with the inlet plane of symmetry in figure 4. The figure also defines the angle θ, which is used throughout this report.

The compressor face total pressures were sensed with a standard scanivalve system which is described in reference 2. The accuracy of each pressure measurement was approximately 0.5 percent of its reading.

The average dynamic pressure at the compressor face, $\overline{q_2}$, was calculated from corrected engine airflow, compressor face area, average compressor face total pressure, and wind tunnel total temperature. Corrected engine airflow was set and measured using the mass flow plug system shown in figure 2 and described in reference 2. Free-stream total pressure, p_{t_0}, was measured with standard wind tunnel instrumentation also described in reference 2.

TEST CONDITIONS AND PROCEDURES

The wind tunnel model was tested at three test conditions that were representative of flight for the YF-12 airplane. The tests generated a range of distortion levels that were representative of those obtained in flight. For all three test conditions, Mach number was set above 2.0, where the inlet operates in the mixed-compression mode. Different values for Mach number, Reynolds number, angle of attack and sideslip, spike position, forward and aft bypass door position, and corrected engine airflow were used for each test. The values for these parameters, which are relevant but not essential to this investigation, are not presented in this report because of their security classification. However, the values are given in figures 166 to 168 of reference 2.

Test conditions were allowed to stabilize before probe measurements were made and remained stable during data acquisition. After the stabilization period, data were obtained with the rake assembly in each of eight positions. The location of each rake referenced to the inlet plane of symmetry is given in table 1. The 64 rake locations obtained in this way were used to acquire 320 total pressure measurements (fig. 5); 320 total pressure measurements were acquired for all three test conditions.

METHOD OF ANALYSIS

Rake Configurations

Different numbers of rakes were used to evaluate the effects of probe number on the calculation of distortion. The subsets of the pressure measurements that were chosen from the 320 probes available are shown in figure 6. The configurations contained 32, 16, eight, seven, six, five, and four rakes. In figure 6, rake 1 of each configuration is alined with the inlet plane of symmetry.

To make sure that the effect of the number of probes on the distortion calculation was fully known, rake orientations that deviated from those shown in figure 6 were also investigated. This was done by selecting as many orientations for each rake as possible from the array of 64 rakes. For example, for a seven-rake configuration, nine orientations could be attained from the 64 available rake positions shown in figure 5. These nine orientations are shown in figure 7.

The angular displacement of the number 1 rake for all the angular orientations is given in table 2 for all of the rake configurations used. Rake spacing for all configurations was as close to equiangularity as possible.

Distortion Descriptors

The effects of probe number on the accuracy of the five distortion descriptors K_θ, K_r, K_a, IDC, and IDT were evaluated in this study, as well as the accuracy of the calculation of average compressor face total pressure, $\overline{p_{t_2}}$. The descriptors are defined and characterized in table 3. Values for each of these parameters were calculated for each rake configuration and angular location shown in table 2. The values were then compared with reference values obtained with 320 probes. The percentage of distortion descriptor error, ε_K, was found for a distortion descriptor K by using the following equation:

$$\varepsilon_K = \frac{K - K_{320}}{K_{320}} 100$$

The percentage of error in $\overline{p_{t_2}}$ was obtained in a similar manner.

RESULTS

Total Pressures Measured at Compressor Face

The 320 total pressures measured at the compressor face for the three test conditions are expressed as a ratio of free-stream total pressure, p_{t_0}, in figures 8 to 10. The resulting values are plotted against angular location, θ, for the five rings shown in figure 4. The angular locations of the centerbody support struts are also shown in the figures. Table 4 presents the values of $\overline{p_{t_2}}/p_{t_0}$ and $\overline{q_2}/p_{t_0}$, along with the values for the five distortion descriptors calculated from the 320-probe arrays for the three test conditions.

Conventional total pressure contours, which show the pressure distribution over the compressor face area, were prepared from the data in figures 8 to 10 and are shown in figures 11 to 13. Values for $\overline{p_{t_2}}/p_{t_0}$, $\left(p_{t_2}/p_{t_0}\right)_{max}$, and $\left(p_{t_2}/p_{t_0}\right)_{min}$ are also included. The locations of the centerbody support struts are shown in figures 8 to 13, since the wake from each strut clearly affected the pressure distribution. In figures 8 to 10, the wake caused a drop in pressure of approximately $\pm 10°$ around the angular location of each strut.

Error in Distortion Descriptors

For each test condition, ε_K was calculated for the five distortion descriptors. The error values for the five descriptors were plotted against the number of rakes and probes for the various angular locations of the different rake configurations (table 2) in figures 14 to 18. To facilitate comparisons with data in previous studies, a distinction is made between the error values obtained when one or more rakes were immersed in the strut wakes and the error values obtained when all the rakes were outside the wakes. This was done because the rakes in most previous studies have been located outside the wake of upstream disturbances. Rakes were considered to be outside the strut wakes when their angular locations were more than 10° away from the strut locations. Some configurations (those with 320, 160, 35, and 25 probes) always had one or more rakes in a wake, however.

For K_θ, K_r, and K_a (figs. 14, 15, and 16), the errors were fairly symmetrically distributed about the reference values. For IDC and IDT (figs. 17 and 18), however, the errors exhibited a bias in the negative direction.

Distortion data are commonly measured with eight-rake/40-probe arrays. The errors in all five distortion descriptors were significant for this configuration, even when all rakes were outside the strut wakes. The maximum errors in K_θ and K_r were approximately $\pm$30 percent; for K_a they were approximately $\pm$20 percent. The error for IDC ranged from 10 percent to -50 percent, and that for IDT from 0 to -40 percent. When fewer probes were used (from 20 to 40), the errors were even greater. The maximum errors were 72 percent for K_θ, -40 percent for K_r, 57 percent for K_a, -70 percent for IDC, and -57 percent for IDT.

To determine whether the error in the calculation of the five distortion descriptors was a function of the angular location of the rake configuration, error values were plotted against the angular location of rake 1 for the eight-rake/40-probe configuration. The results are shown in figures 19(a) to 19(e). The angular location of the rakes with respect to the struts is indicated in figure 20.

As figure 19 shows, when four of the eight rakes are directly behind struts (that is, when rake 1 is at an angular location of 0°), there are considerable negative errors in all five descriptors. However, the error values obtained are not necessarily the largest. As rake 1 moves clockwise and the rakes move out of the strut wakes, the error in all the descriptors tends to increase, up to an angle of approximately 35°. Beyond this angle, the error of all the descriptors tends to decrease to the value obtained when rake 1 was at the 0° location. These trends are only general, however, for several exceptions to the trend are apparent in the three test conditions used.

Error in Average Total Pressure at Compressor Face

Error bands for the calculation of $\overline{p_{t_2}}$ as a function of the number of rakes and and probes are presented in figure 21. The error in $\overline{p_{t_2}}$ was generally less than ± 1 percent when 40 probes were used; for fewer probes, errors up to ± 2 percent were obtained.

Effect of Number of Probes on Total Pressure Patterns

Total pressure patterns were mapped using the pressure measurements from 64, eight, and seven rakes. The maps are shown along with their distortion values in figures 22 to 24.

The maps constructed from eight and seven rakes show the general patterns of pressure distribution. However, the maps constructed from 64 rakes show the patterns in much more detail.

SUMMARY OF RESULTS

A study was performed to determine the effects of the number and position of total pressure probes on the calculation of five steady state compressor face distortion descriptors and average compressor face total pressure. This study used sets of 320 total pressures that were obtained from wind tunnel tests made at three test conditions on a one-third-scale model of a YF-12 airplane mixed-compression inlet. The three test conditions were representative of flight conditions above Mach 2.0. The pressures were measured at the inlet compressor face with a special rotating rake apparatus.

This study showed that large errors can result in the calculation of distortion descriptors even with a number of equal-area-weighted total pressure probes that has been thought to be adequate in the past. For an eight-rake/40-probe configuration, the errors obtained in distortion descriptors for several rake locations were as follows:

1. For one circumferential distortion descriptor (K_θ), errors as large as ± 30 percent were obtained, and for another (IDC), maximum errors of 10 to -50 percent were obtained.

2. A radial distortion descriptor (K_r) showed errors of ± 30 percent.

3. A descriptor (K_a) that combined the circumferential distortion descriptor K_θ, with the radial descriptor, K_r, showed maximum errors of ± 20 percent.

4. Errors in the maximum-minus-minimum-over-average-pressure distortion descriptor, IDT, showed errors from 0 to -40 percent.

The use of fewer probes (from 20 to 40) resulted in errors for all the descriptors of 40 percent or more.

The calculation of average total pressure was also affected by probe number and location, although not to the same extent as the distortion descriptors. For the eight-rake/40-probe configuration, the errors were less than ± 1 percent. With fewer probes (from 20 to 40), the error increased to ± 2 percent.

Maps of total pressure at the compressor face that were constructed using the probes on eight or seven rakes showed the general pressure pattern, but failed to show the detail apparent in maps created using 64 rakes.

Dryden Flight Research Center
National Aeronautics and Space Administration
Edwards, Calif., November 17, 1978

REFERENCES

1. Schweikhard, William G.: Test Techniques, Instrumentation, and Data Processing. Distortion Induced Engine Instability, AGARD-LS-72, Oct. 1974, pp. 6-16–6-43.

2. Anderson, G. Thomas; Martin, Robert K.; and Shibata, Harry H.: 1/3 Scale Inlet Model Test Results. Vol. I - Test Definition and Steady State Data Presentation. NASA CR-114702, 1974.

3. Bauer, Carol A.; Mackall, Karen G.; Stoll, Frederick; and Tremback, Jeffrey W.: Comparison of Flight and Wind Tunnel Model Instantaneous Distortion Data From a Mixed-Compression Inlet. YF-12 Experiments Symposium. NASA CP-2054, Vol. 3, 1978, pp. 295-375.

4. Arnaiz, Henry H.; Brownlow, James D.; and Albers, James A.: A Comparison of Steady-State Performance Among a Flight Inlet on a YF-12 Airplane and Two Wind Tunnel Models Using Statistical Techniques. YF-12 Experiments Symposium. NASA CP-2054, Vol. 3, 1978, pp. 187-292.

5. Burcham, Frank W., Jr.; Montoya, Earl J.; and Lutschg, Phillip J.: Description of YF-12C Airplane, Propulsion System, and Instrumentation for Propulsion Research Flight Tests. NASA TM X-3099, 1974.

TABLE 1. —ANGULAR RAKE POSITION FOR EIGHT ORIENTATIONS OF ROTATING RAKE ASSEMBLY

Rake assembly position	Rake 1	Rake 2	Rake 3	Rake 4	Rake 5	Rake 6	Rake 7	Rake 8
	Location of each rake, deg							
1	15	60	105	150	195	240	285	330
2	20	65	110	155	200	245	290	335
3	27.5	72.5	117.5	162.5	207.5	252.5	297.5	342.5
4	35	80	125	170	215	260	305	350
5	42.5	87.5	132.5	177.5	222.5	267.5	312.5	357.5
6	45	90	135	180	225	270	315	0
7	50	95	140	185	230	275	320	5
8	57.5	102.5	147.5	192.5	237.5	282.5	327.5	12.5

TABLE 2. —ANGULAR LOCATION FOR RAKE CONFIGURATIONS USED IN DISTORTION DESCRIPTOR EVALUATION

Rake configuration		Approximate included angle between rakes (fig. 6), deg	Angular location of rake 1 for each rake configuration, deg
Number of rakes	Number of probes		
64	320	5.625	0
32	160	11.25	0, 5
16	80	22.5	0, 5, 12.5, 15
8	40	45	0, 5, 12.5, 15, 20, 27.5, 35, 42.5
7	35	51.43	0, 5, 12.5, 15, 20, 27.5, 35, 42.5, 45
6	30	60	0, 5, 12.5, 15, 20, 27.5, 35, 42.5, 45, 50, 57.5
5	25	72	0, 5, 12.5, 15, 20, 27.5, 35, 42.5, 45, 50, 57.5, 60
4	20	90	0, 5, 12.5, 15, 20, 27.5, 35, 42.5, 45, 50, 57.5, 60, 65, 72.5, 80, 87.5

TABLE 3. —DEFINITION OF DISTORTION DESCRIPTORS

Distortion descriptor	Type of distortion described	Definitions
K_θ	Circumferential	$K_\theta = \dfrac{\sum_{i=1}^{NP} K_{\theta_i}/R_i}{\sum_{i=1}^{NP} 1/R_i}$ where $K_{\theta_i} = \dfrac{1}{\overline{q_2}}\sqrt{A_i^2 + B_i^2}$ $A_i = \dfrac{1}{180}\sum_{j=1}^{NR} p_{t_{2_{i,j}}} \Delta\theta_j \cos\theta_j$ $B_i = \dfrac{1}{180}\sum_{j=1}^{NR} p_{t_{2_{i,j}}} \Delta\theta_j \sin\theta_j$
K_r	Radial	$K_r = \dfrac{\sum_{i=1}^{NP} K_{r_i}/R_i^{2.8}}{\sum_{i=1}^{NP} 1/R_1^{2.8}}$ where $K_{r_i} = \dfrac{1}{\overline{q_2}}\left\lvert \overline{p_{t_2}} - \overline{p_{t_{2_i}}} \right\rvert$ $\overline{p_{t_{2_i}}}$ = Ring average total pressure
K_a	Combined circumferential and radial	$K_a = K_\theta + K_r$
IDC	Circumferential	$IDC = \text{Maximum}\left[\frac{1}{2}\left(IDC_1 + IDC_2\right), \frac{1}{2}\left(IDC_4 + IDC_5\right)\right]$ where $IDC_i = \left(\overline{p_{t_{2_i}}} - p_{t_{2_{i,j_{min}}}}\right)/\overline{p_{t_2}}$
IDT	Combined	$IDT = \dfrac{\left(p_{t_{2_{i,j}}}\right)_{max} - \left(p_{t_{2_{i,j}}}\right)_{min}}{\overline{p_{t_2}}}$

TABLE 4. —COMPRESSOR FACE TOTAL PRESSURE PARAMETERS CALCULATED FROM 320-PROBE ARRAY AND p_{t_0} FOR TEST CONDITIONS

Test condition	$\overline{p_{t_2}}/p_{t_0}$	$\overline{q_2}/p_{t_0}$	K_θ	K_r	K_a	IDC	IDT	p_{t_0}, N/m^2
1	0.852	0.0941	0.319	0.291	0.609	0.0804	0.245	1.354×10^5
2	0.780	0.0459	0.411	0.368	0.779	0.0551	0.188	1.354
3	0.803	0.0453	0.354	0.349	0.703	0.0321	0.130	1.354

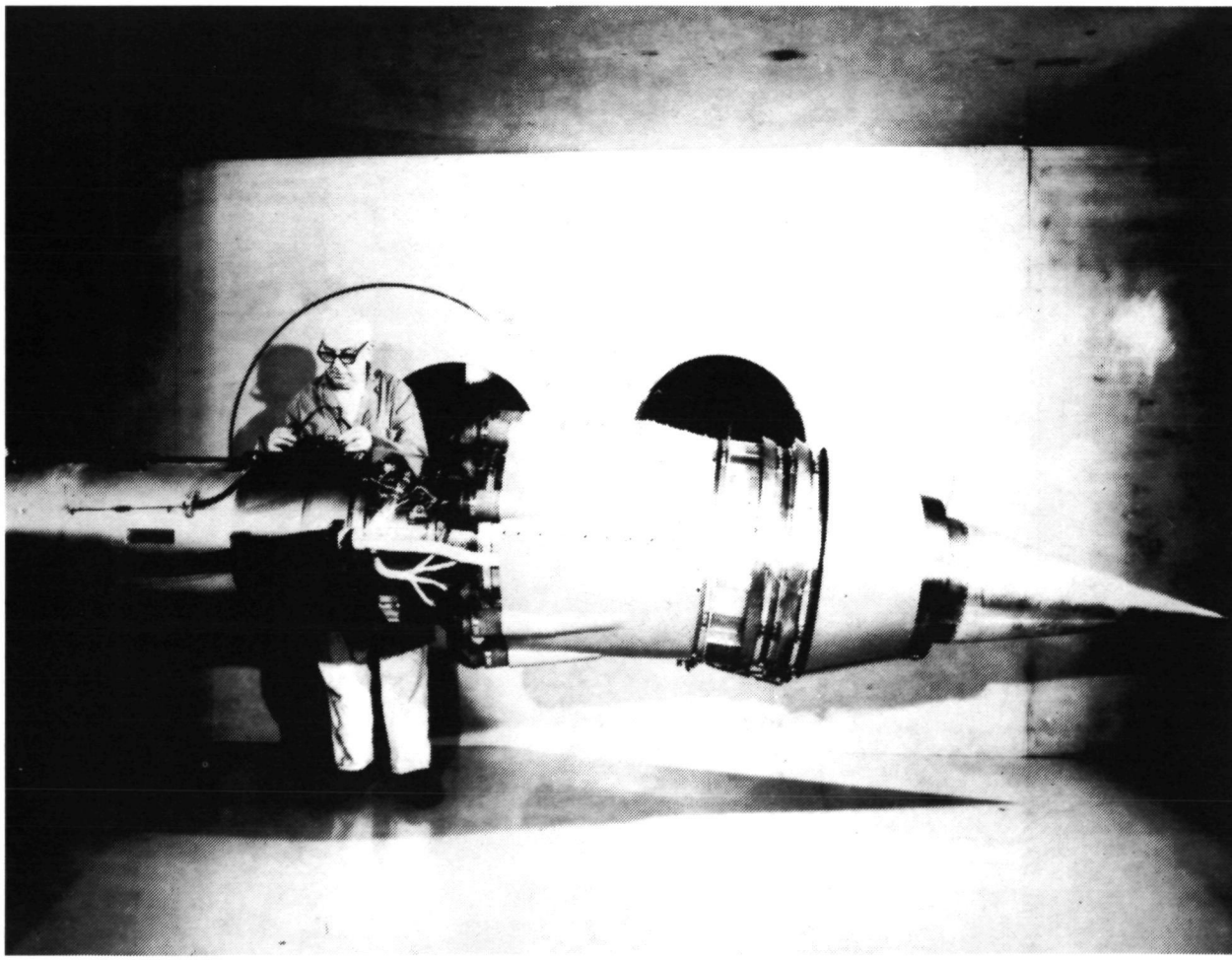

Figure 1. One-third-scale inlet model mounted in Ames 8- by 7- Foot Supersonic Test Section.

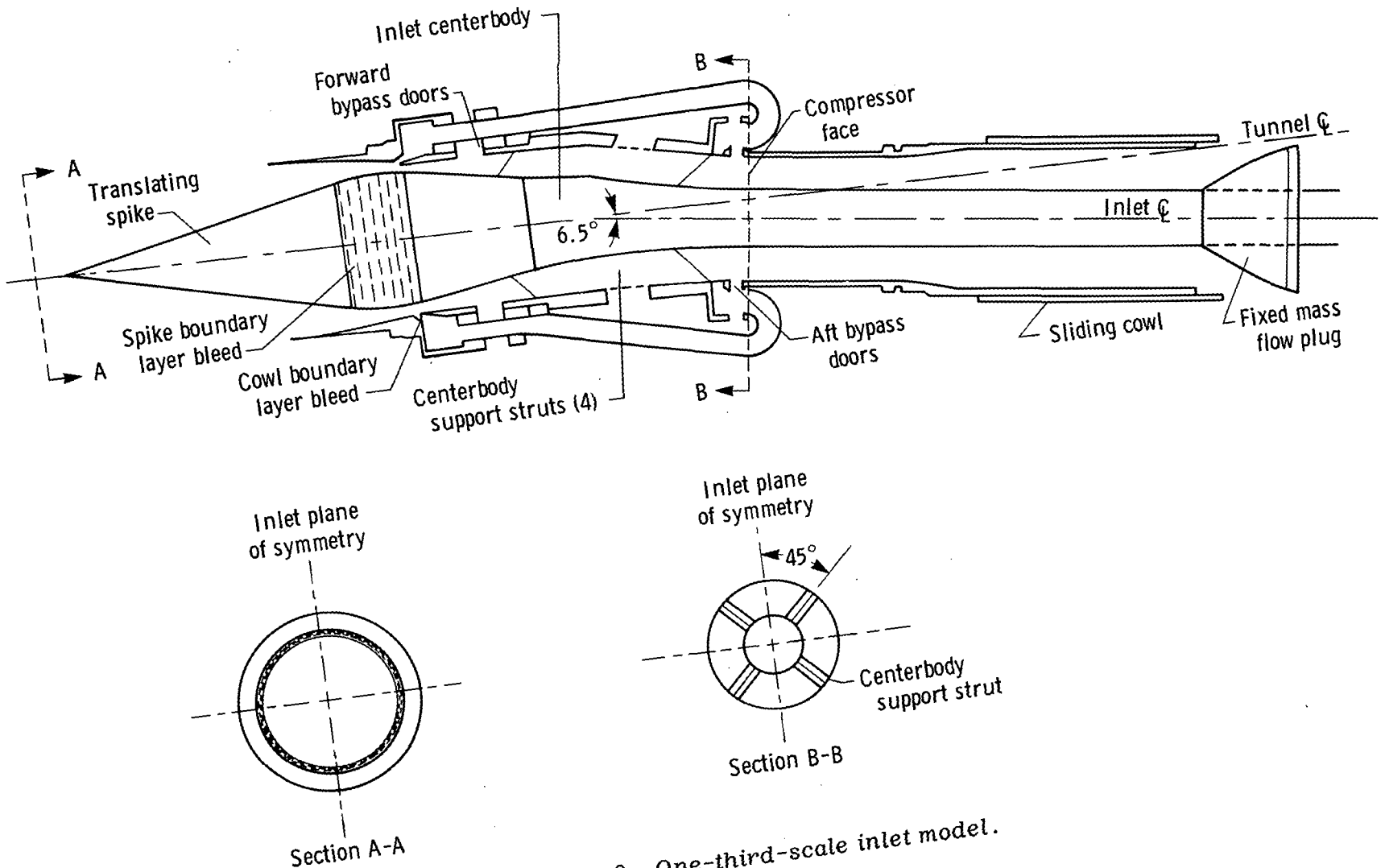

Figure 2. One-third-scale inlet model.

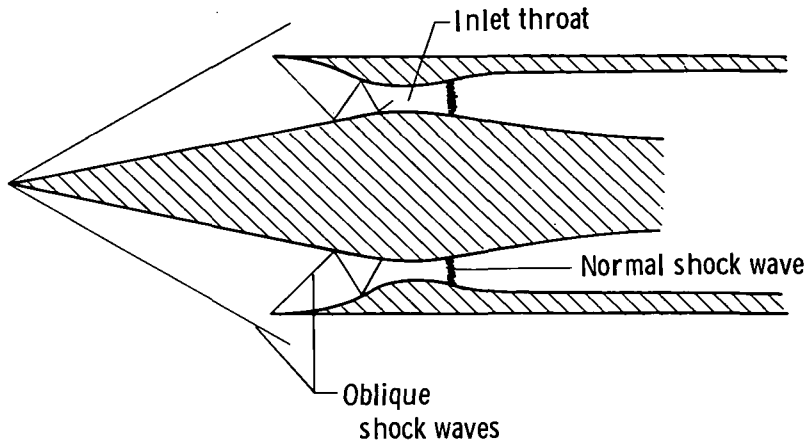

Figure 3. Shock system associated with mixed-compression inlet.

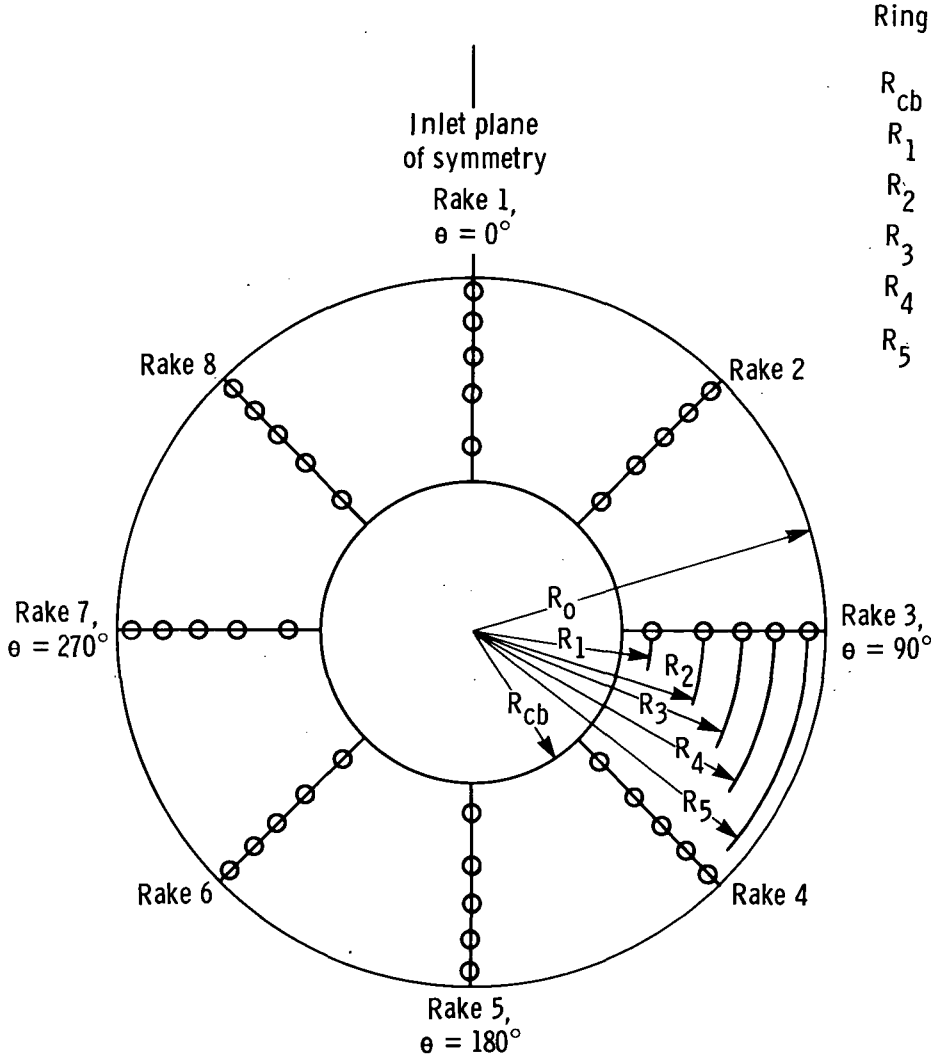

Figure 4. Rotating 40-probe rake assembly looking downstream.

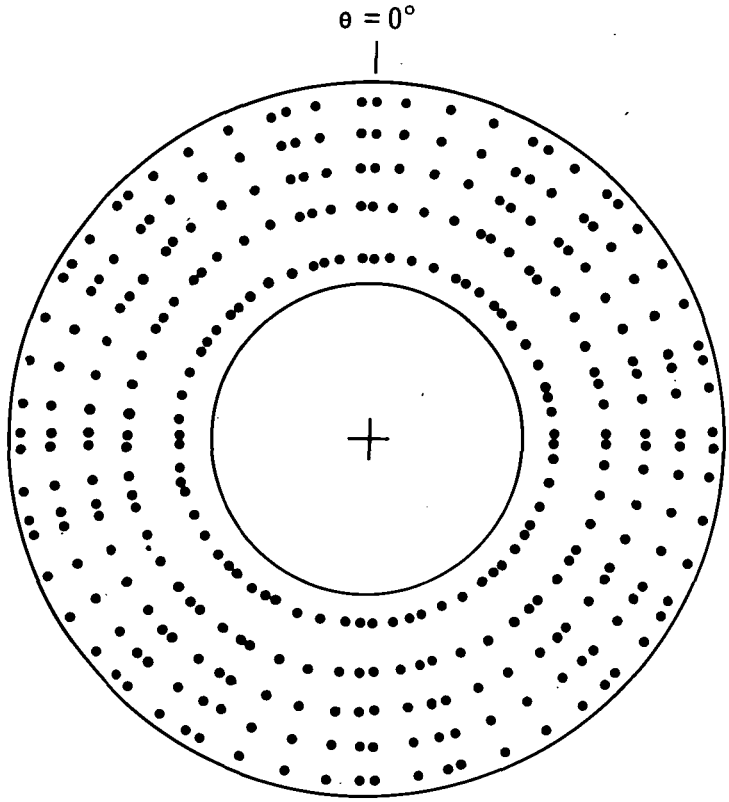

Figure 5. The 64-rake/320-probe pressure array obtained by rotating eight-rake apparatus through eight angular positions (table 1).

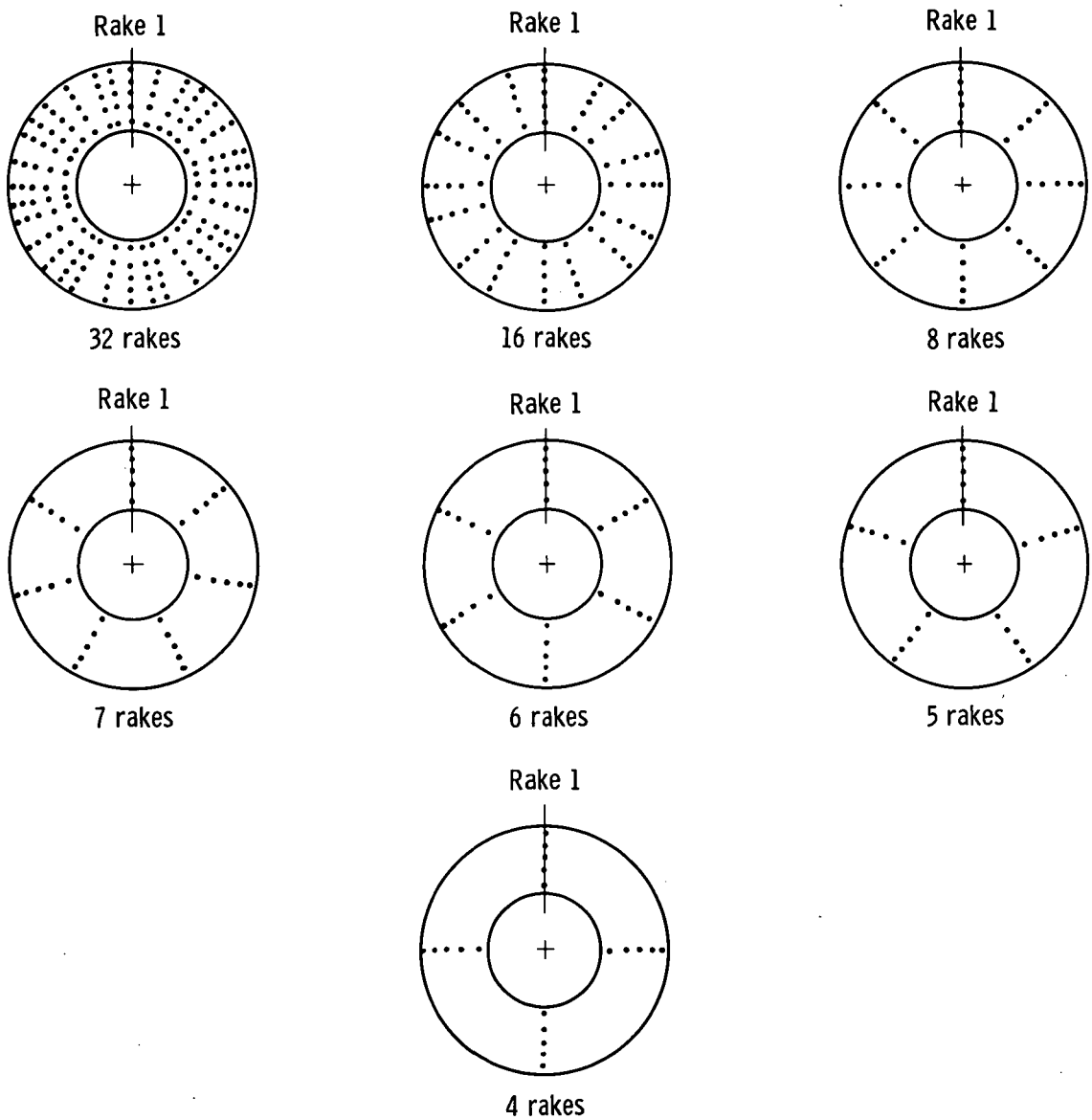

Figure 6. Simulated rake configurations obtained by selecting subsets of 64-rake/320-probe array (fig. 5).

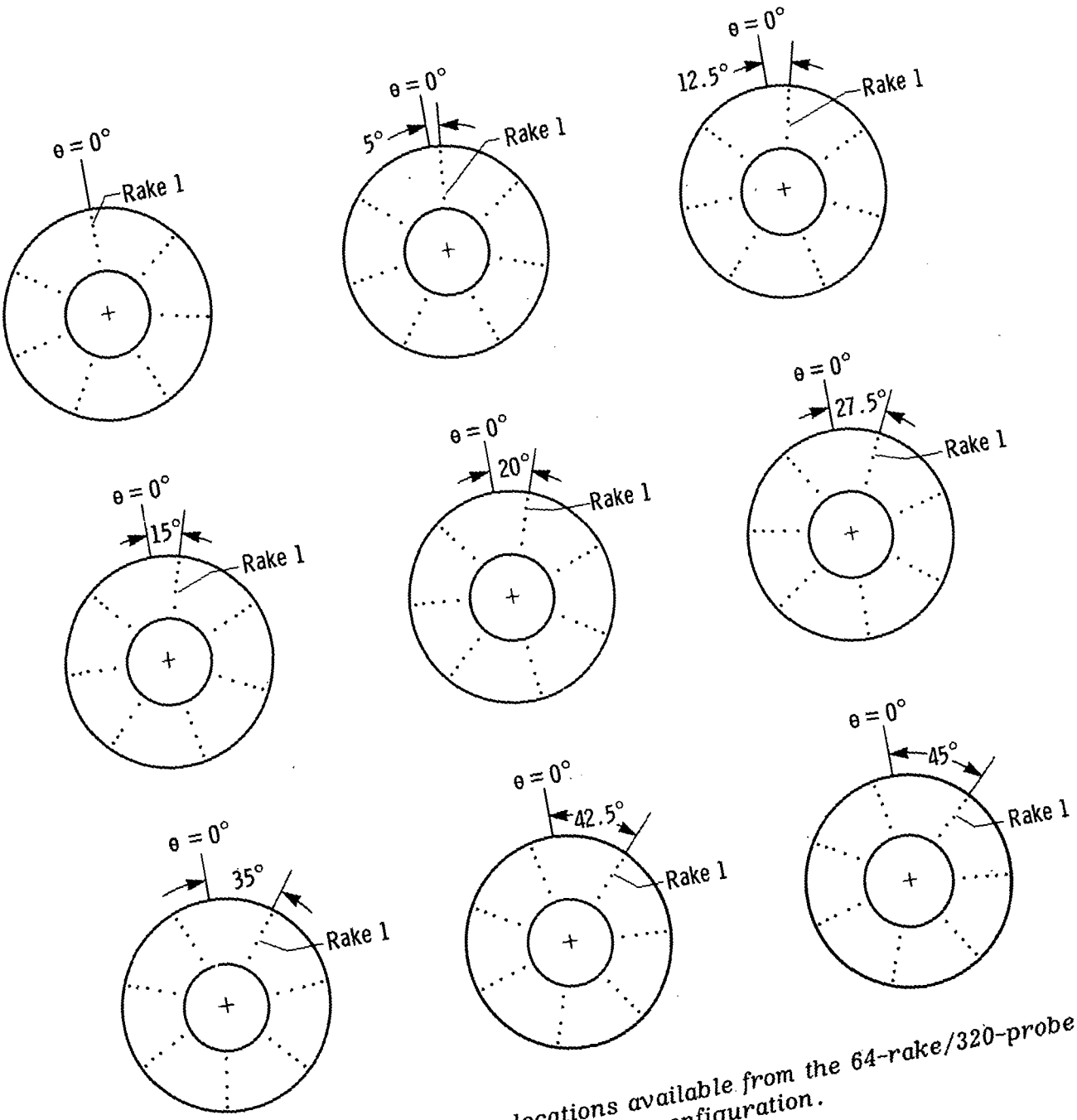

Figure 7. Different angular locations available from the 64-rake/320-probe array (fig. 5) for seven-rake/35-probe configuration.

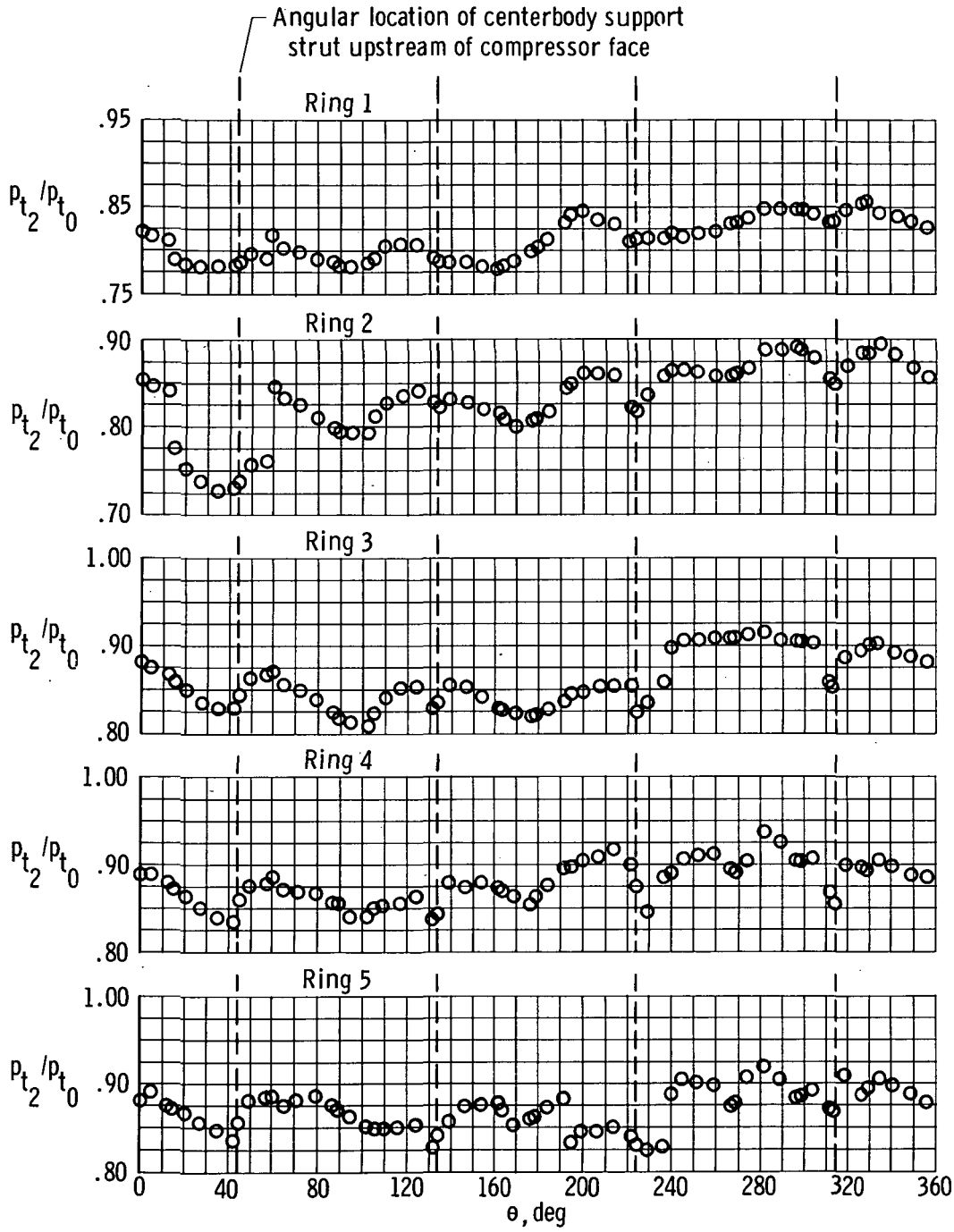

Figure 8. Variation of compressor face total pressure with radial and angular location for test condition 1 using 320-probe array.

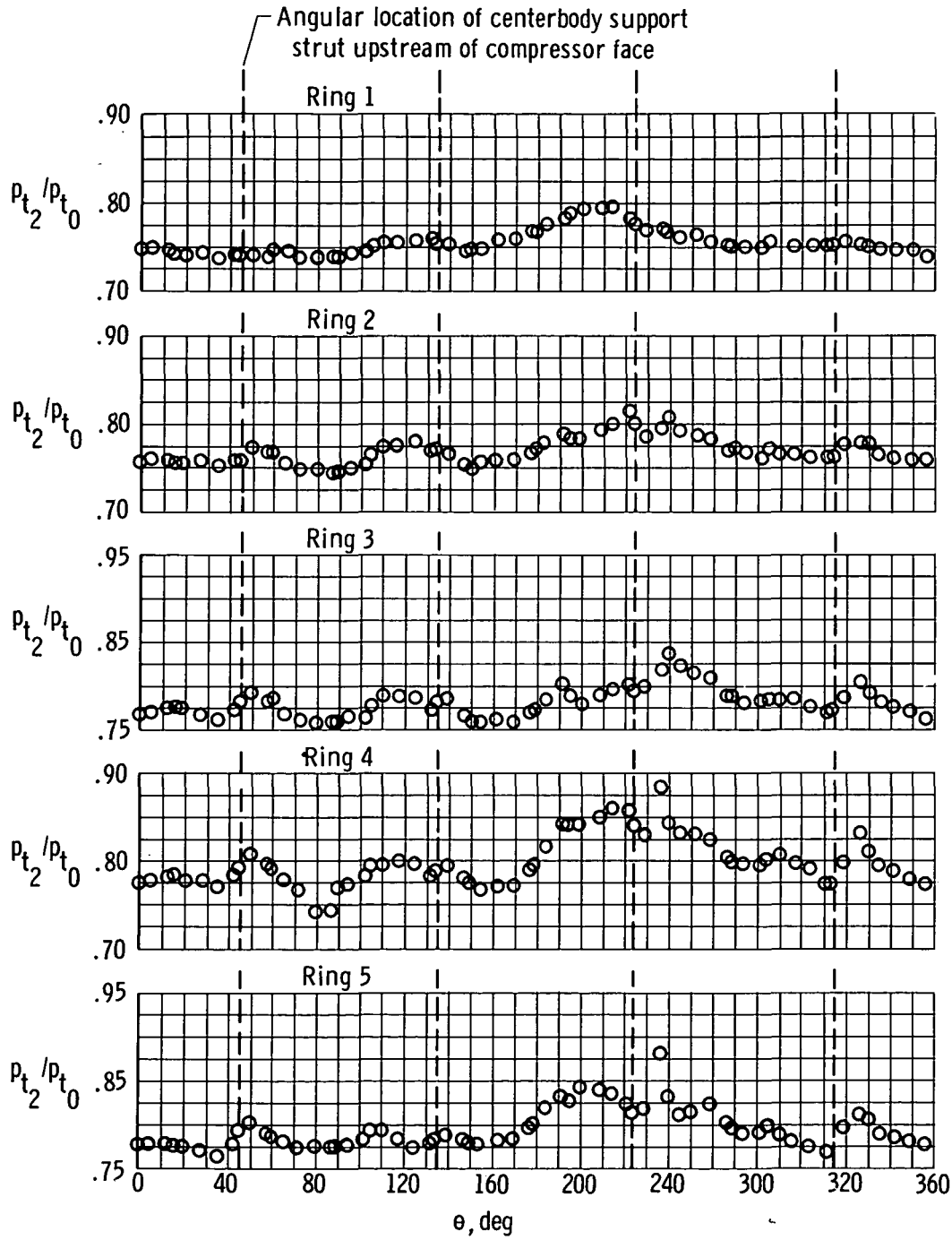

Figure 9. Variation of compressor face total pressure with radial and angular location for test condition 2 using 320-probe array.

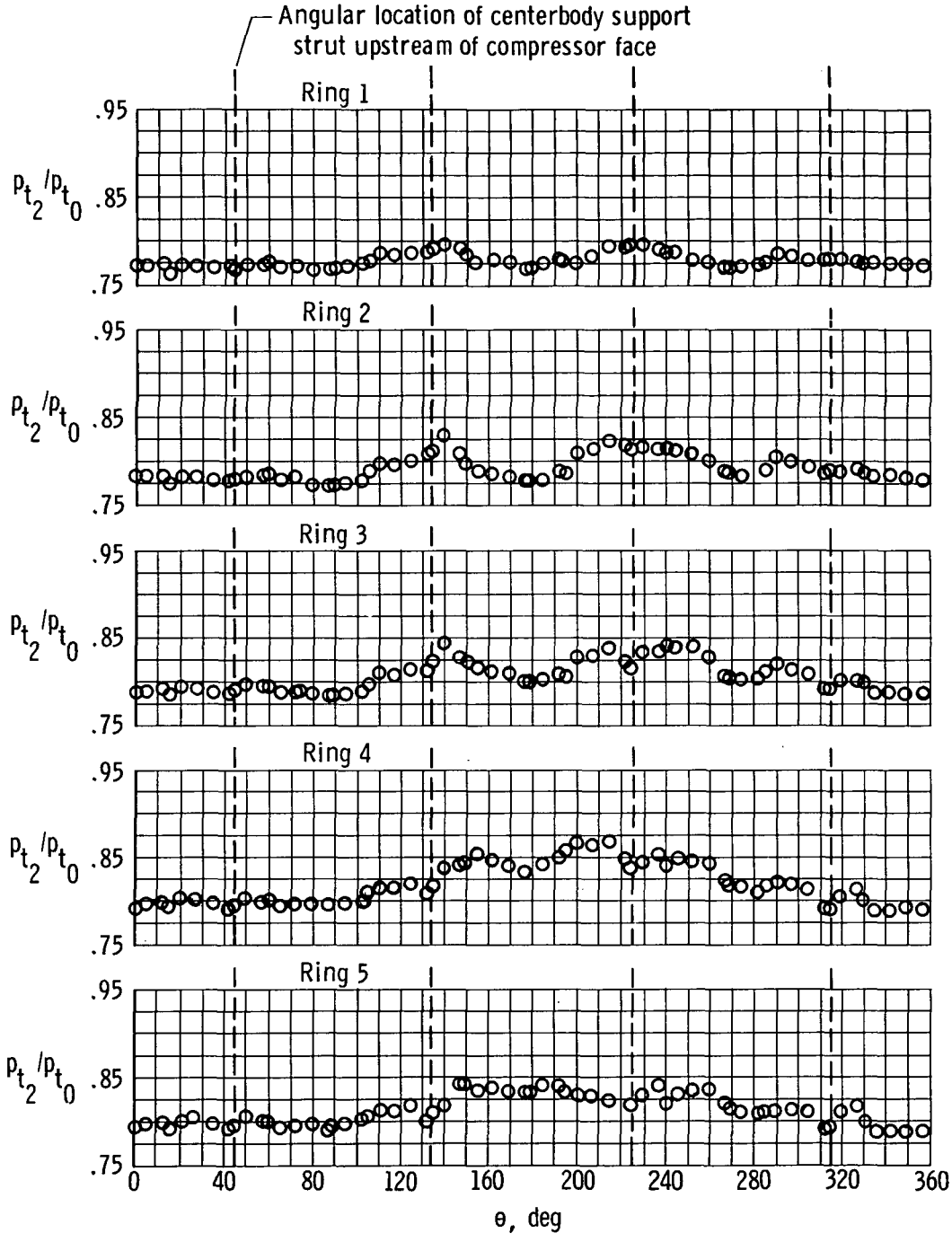

Figure 10. Variation of compressor face total pressure with radial and angular location for test condition 3 using 320-probe array.

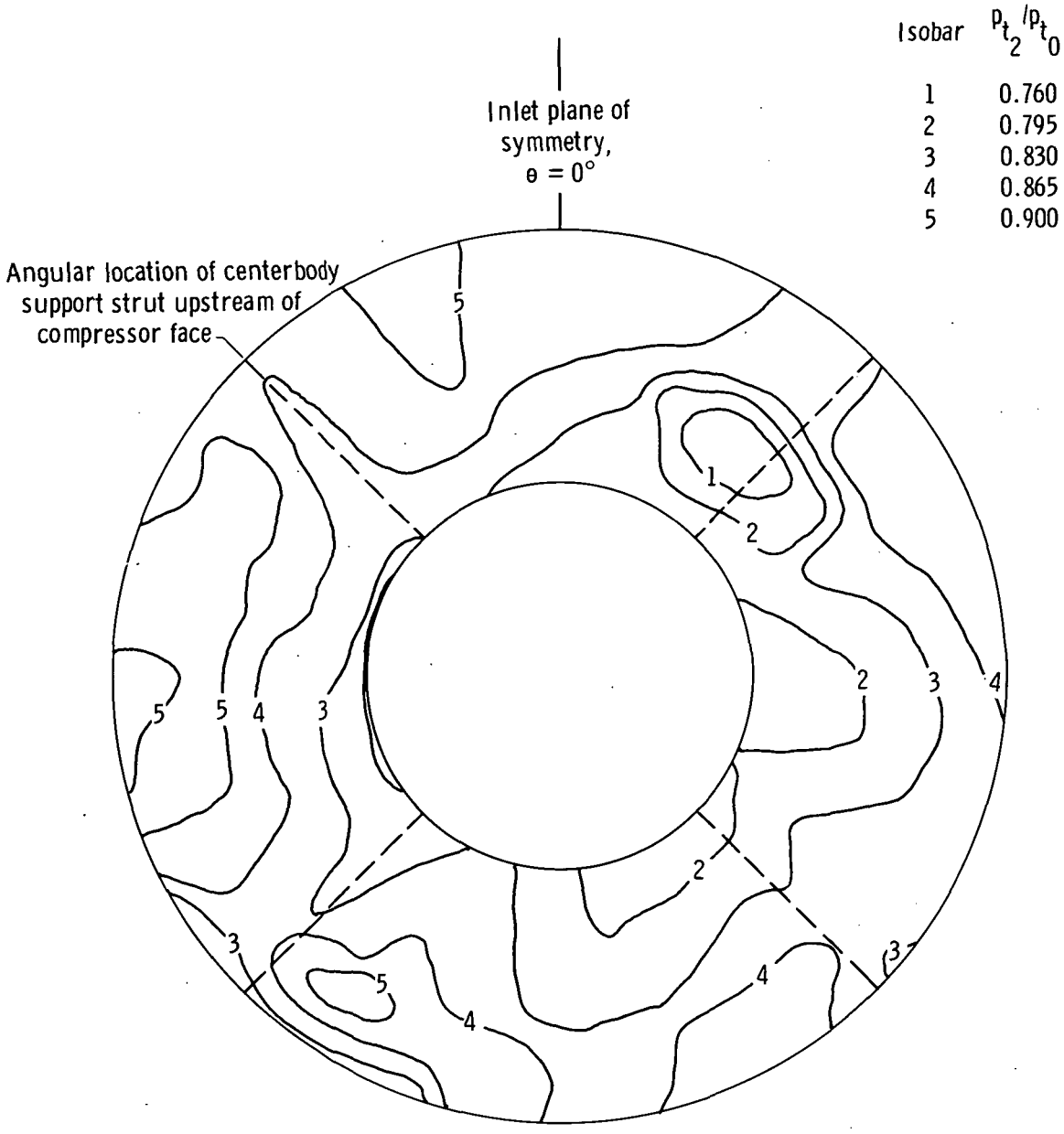

Figure 11. Pattern of compressor face total pressure for test condition 1 and 320-probe array. $\overline{p_{t_2}/p_{t_0}} = 0.852$; $\left(p_{t_2}/p_{t_0}\right)_{max} = 0.938$; $\left(p_{t_2}/p_{t_0}\right)_{min} = 0.729$.

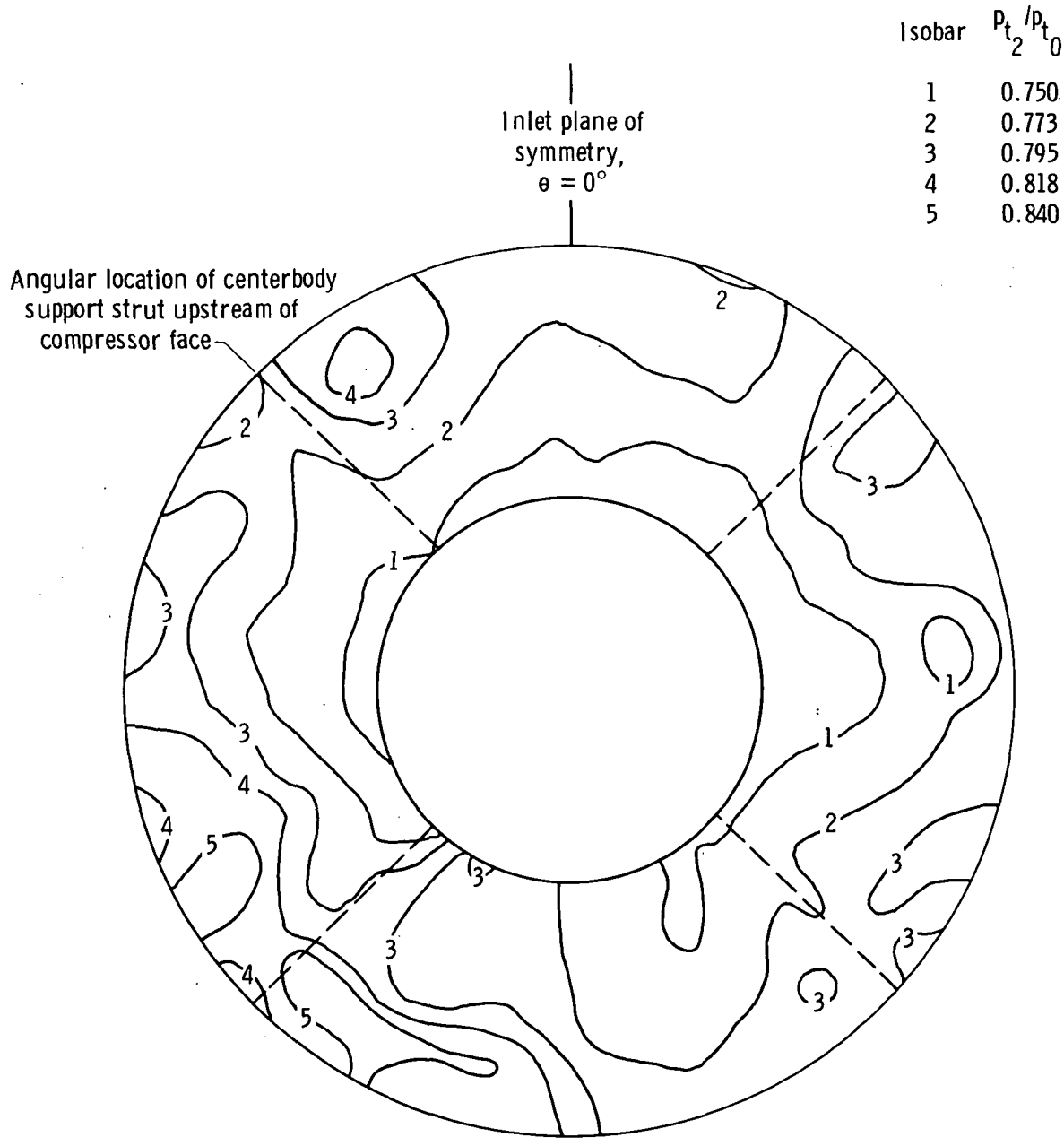

Figure 12. Pattern of compressor face total pressure for test condition 2 and 320-probe array. $\overline{p_{t_2}/p_{t_0}} = 0.780$; $\left(p_{t_2}/p_{t_0}\right)_{max} = 0.885$; $\left(p_{t_2}/p_{t_0}\right)_{min} = 0.738$.

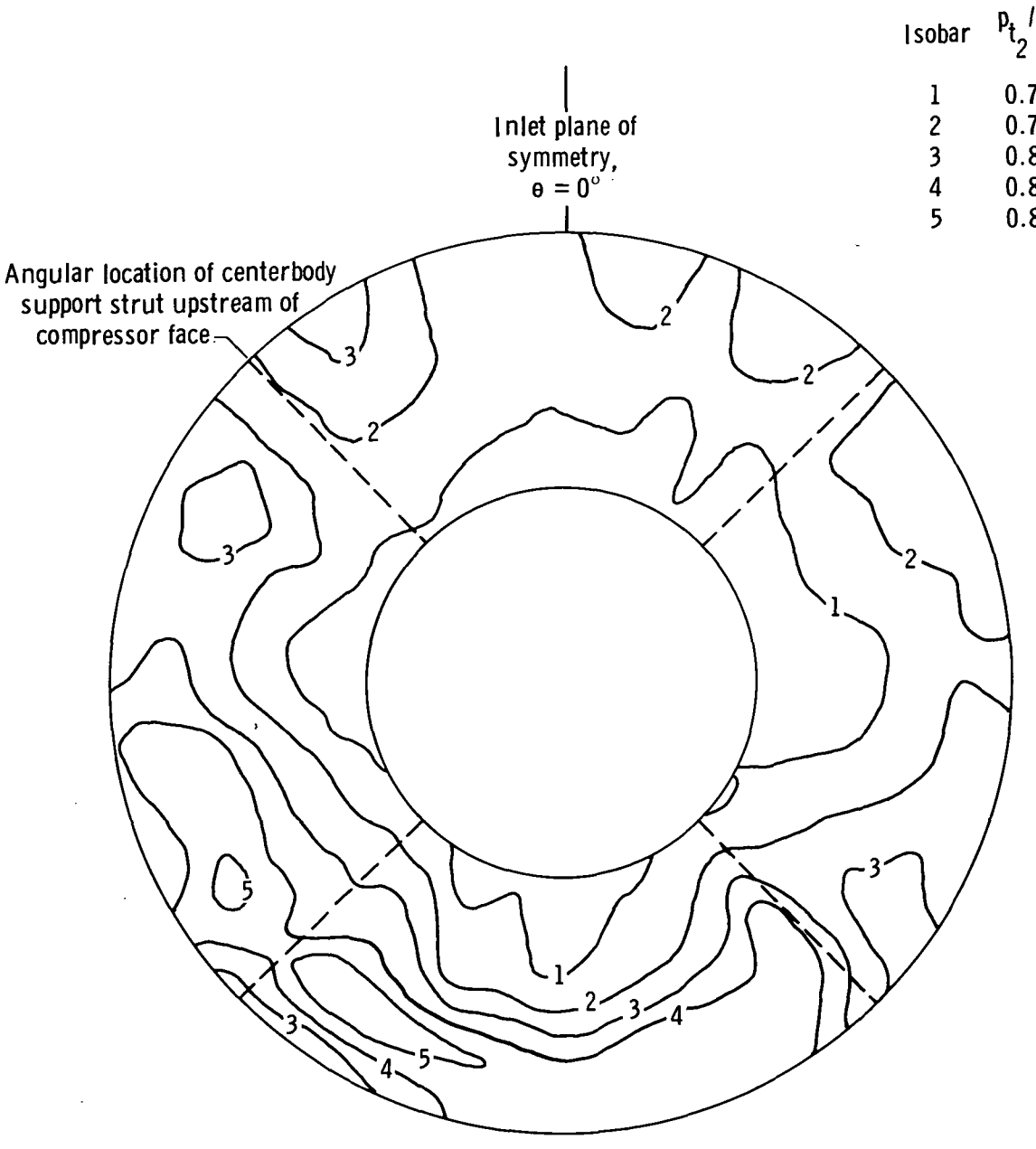

Figure 13. Compressor face total pressure map for test condition 3 and 320-probe array. $\overline{p_{t_2}/p_{t_0}} = 0.803$; $\left(p_{t_2}/p_{t_0}\right)_{max} = 0.869$; $\left(p_{t_2}/p_{t_0}\right)_{min} = 0.765$.

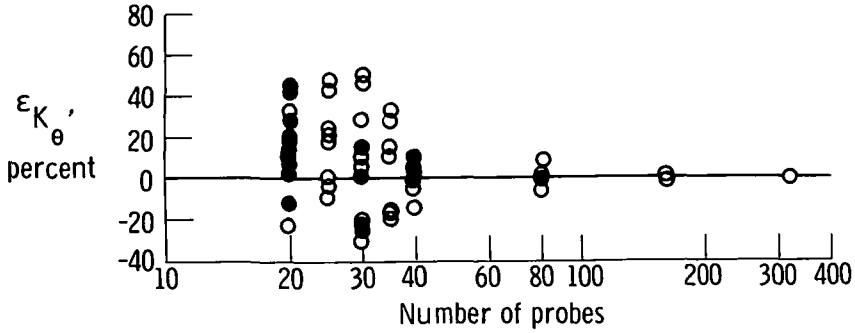

(a) Test condition 1, $K_{\theta_{320}} = 0.319$.

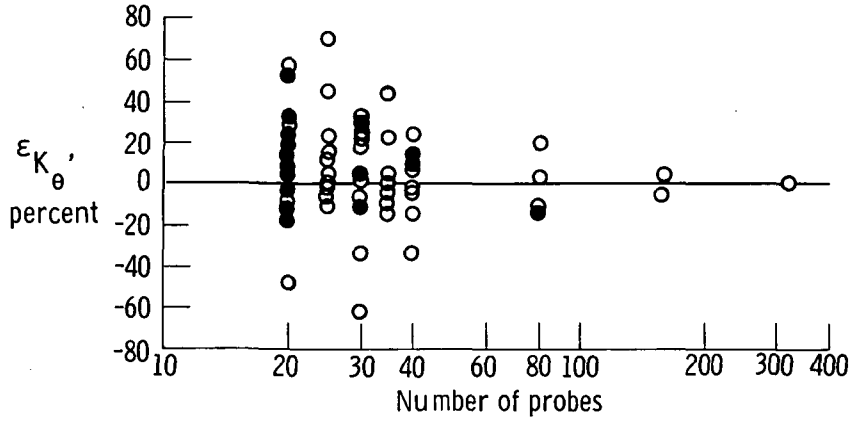

(b) Test condition 2, $K_{\theta_{320}} = 0.411$.

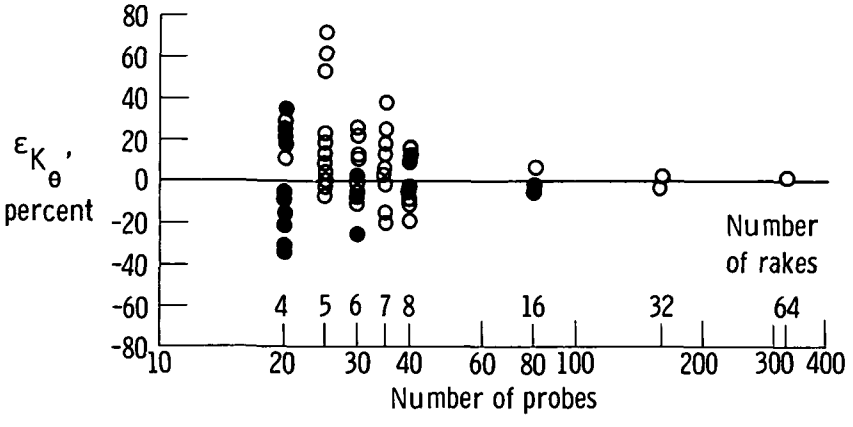

(c) Test condition 3, $K_{\theta_{320}} = 0.354$.

Figure 14. Variation in error of distortion descriptor K_θ with number of probes and rakes for three test conditions. Solid symbols denote that no rakes were in strut wake.

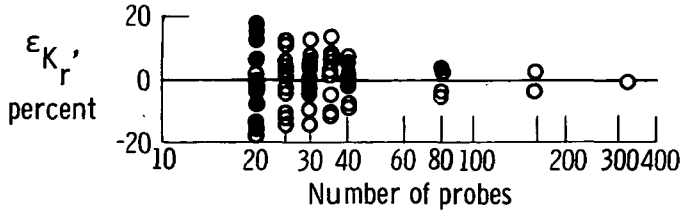

(a) Test condition 1, $K_{r_{320}} = 0.291$.

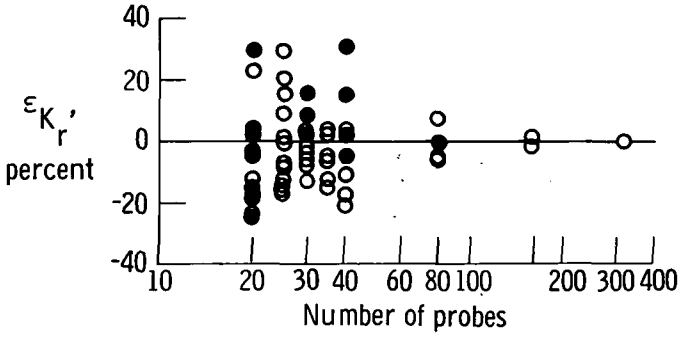

(b) Test condition 2, $K_{r_{320}} = 0.368$.

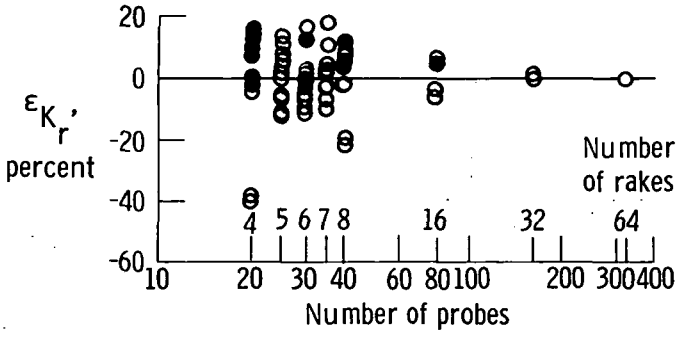

(c) Test condition 3, $K_{r_{320}} = 0.349$.

Figure 15. Variation in error of distortion descriptor K_r with number of probes and rakes for three test conditions. Solid symbols denote that no rakes were in strut wake.

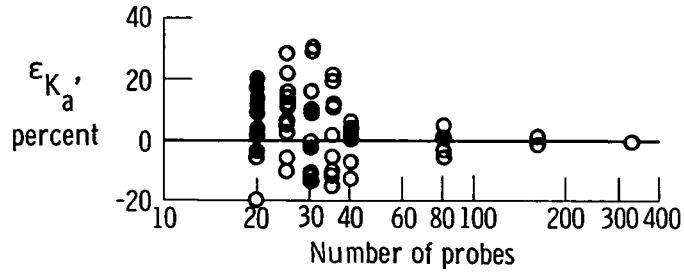

(a) Test condition 1, $K_{a_{320}} = 0.609$.

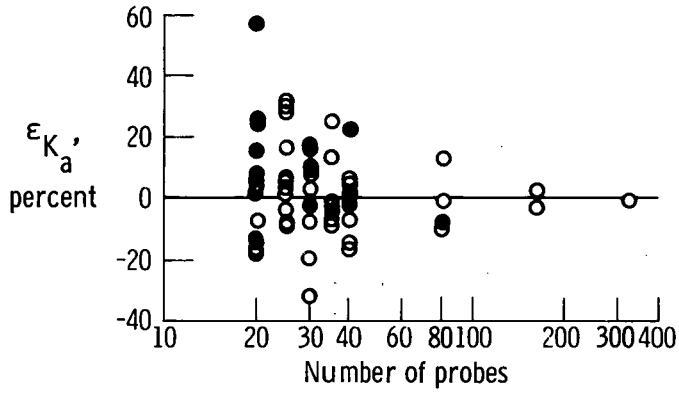

(b) Test condition 2, $K_{a_{320}} = 0.779$.

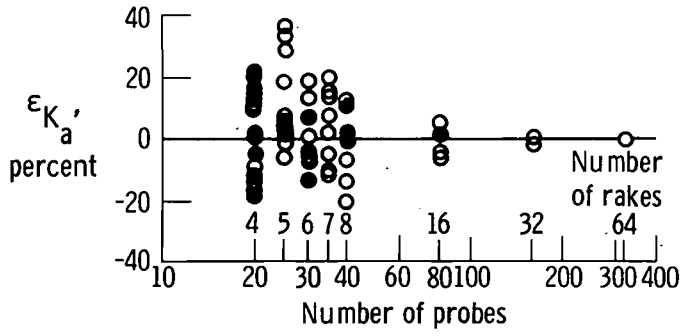

(c) Test condition 3, $K_{a_{320}} = 0.703$.

Figure 16. Variation in error of distortion descriptor K_a with number of probes and rakes for three test conditions. Solid symbols denote that no rakes were in strut wake.

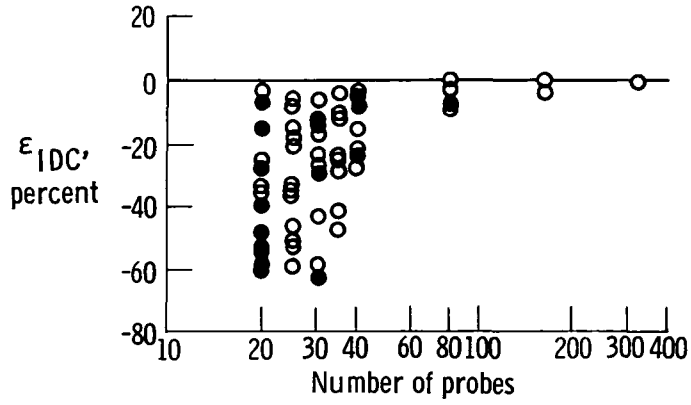

(a) Test condition 1, $IDC_{320} = 0.0804$.

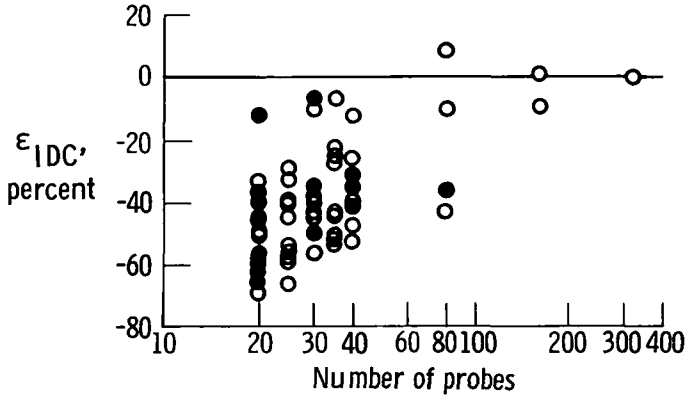

(b) Test condition 2, $IDC_{320} = 0.0551$.

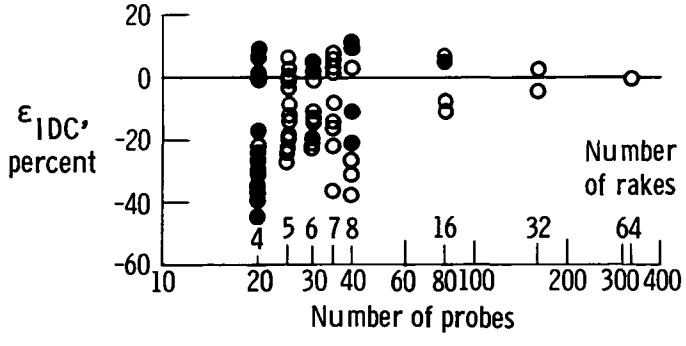

(c) Test condition 3, $IDC_{320} = 0.0321$.

Figure 17. Variation in error of distortion descriptor IDC with number of probes and rakes for three test conditions. Solid symbols denote that no rakes were in strut wake.

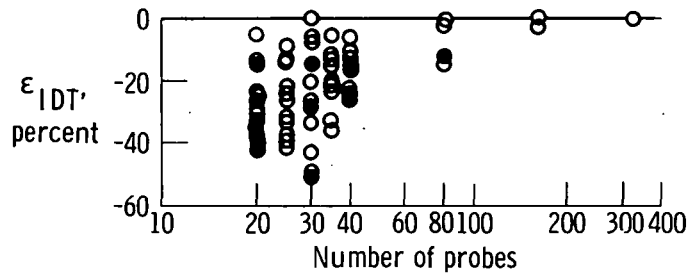

(a) Test condition 1, $IDT_{320} = 0.245$.

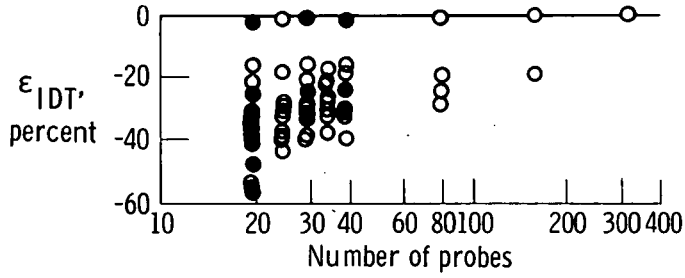

(b) Test condition 2, $IDT_{320} = 0.188$.

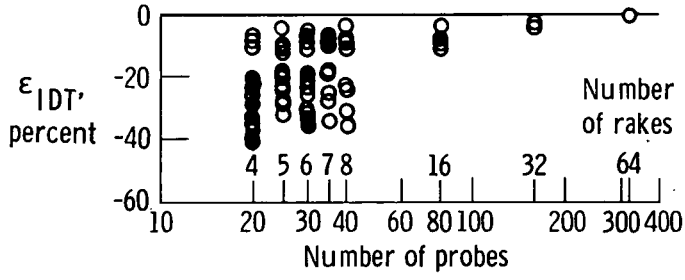

(c) Test condition 3, $IDT_{320} = 0.130$.

Figure 18. Variation in error of distortion descriptor IDT with number of probes and rakes for three test conditions. Solid symbols denote that no rakes were in strut wake.

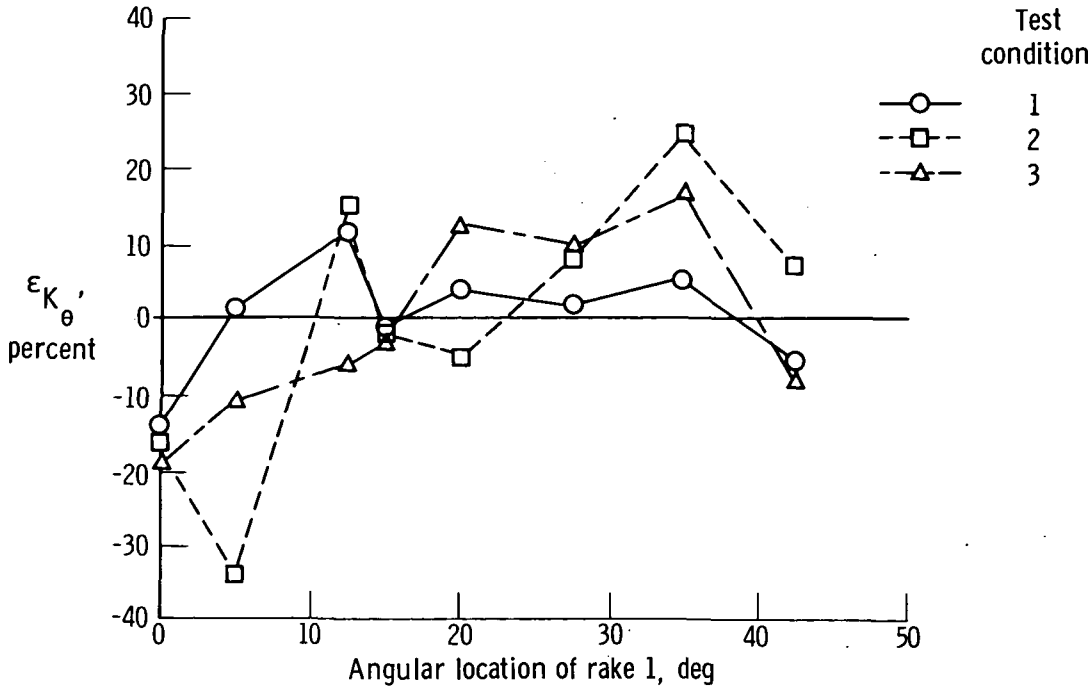

(a) K_θ.

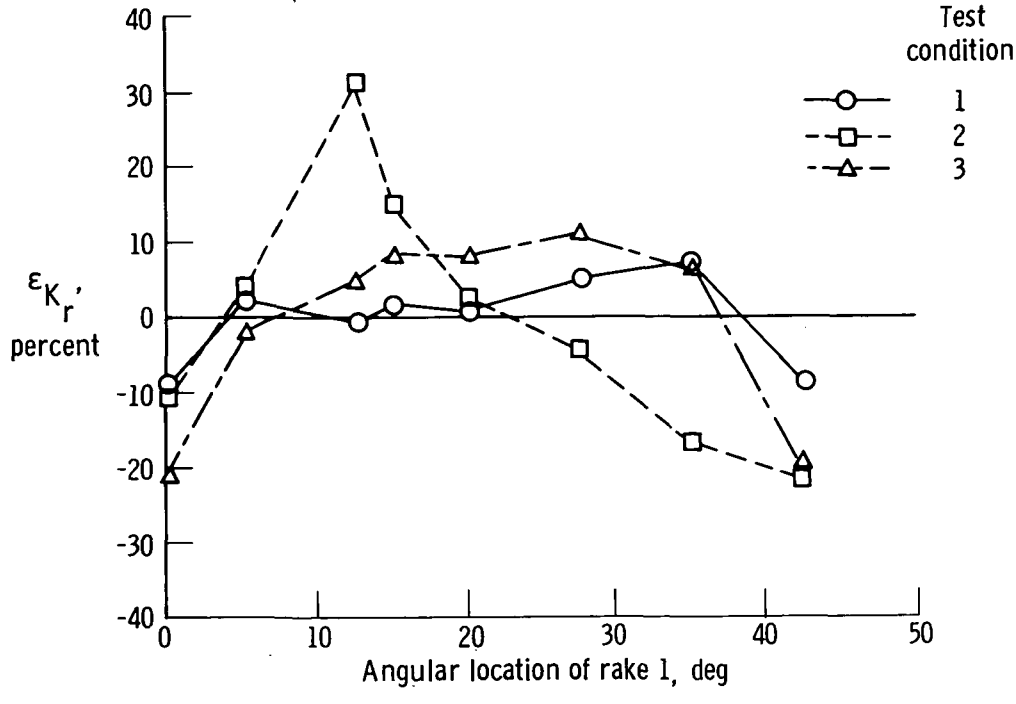

(b) K_r.

Figure 19. Distortion descriptor error as a function of angular location of rake 1 for eight-rake/40-probe configuration at three test conditions.

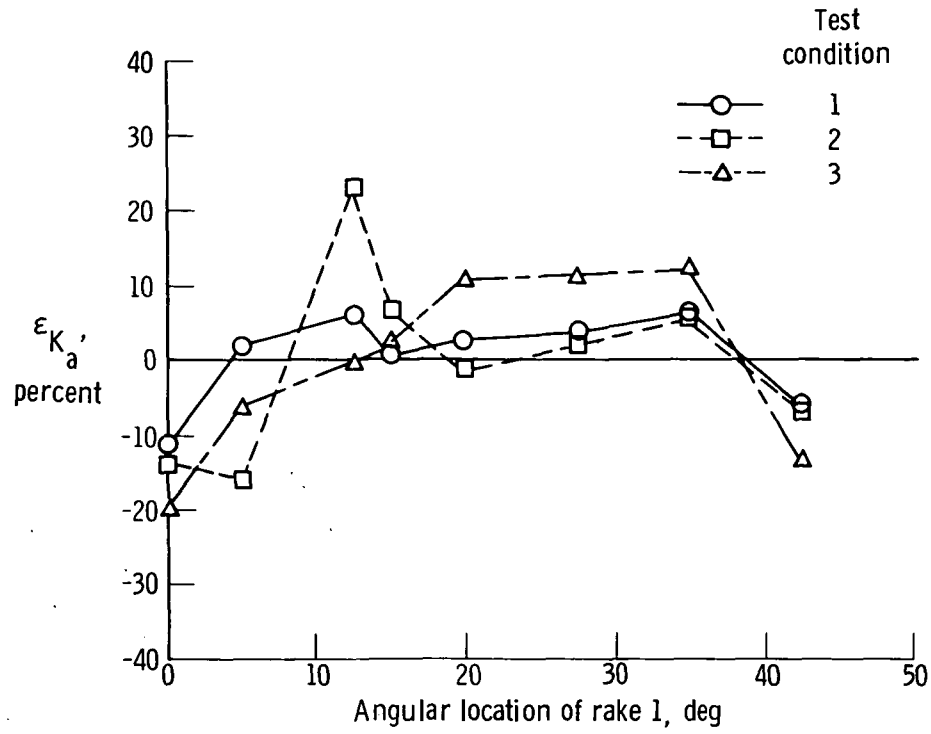

(c) K_a.

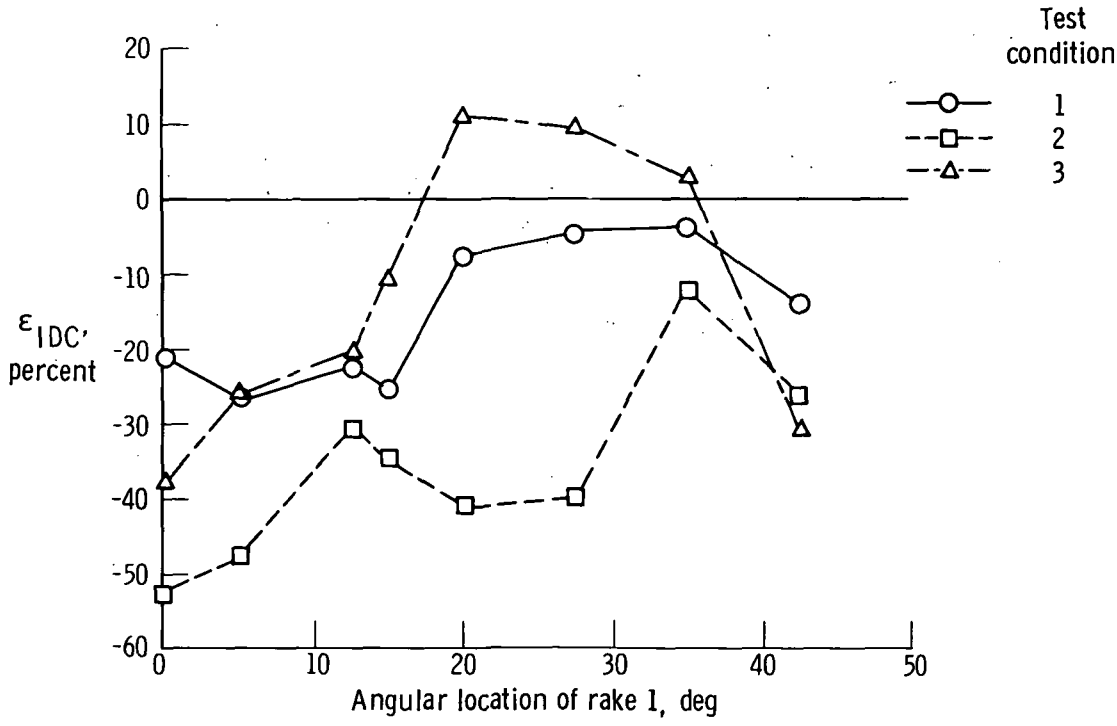

(d) IDC.

Figure 19. Continued.

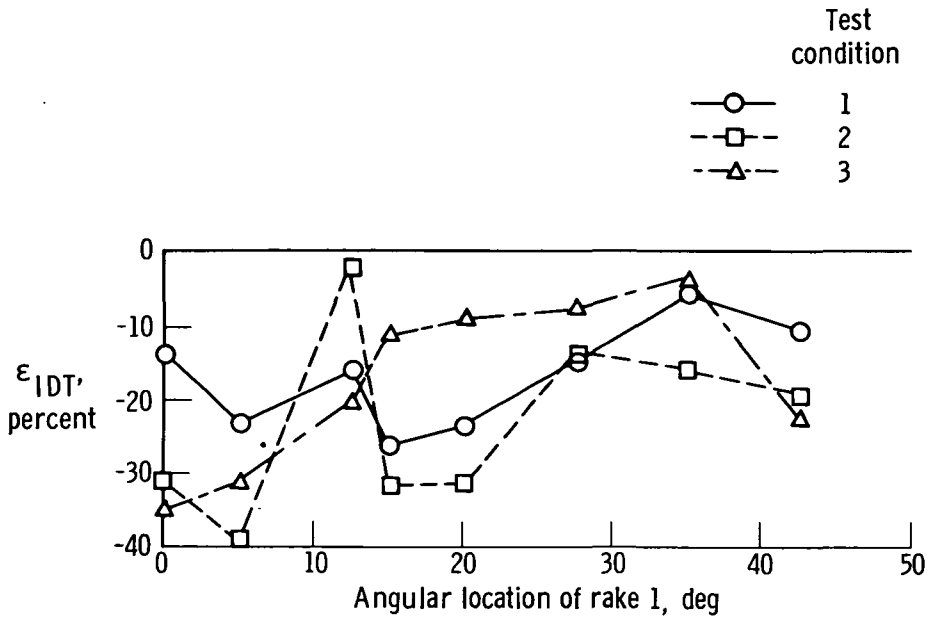

(e) IDT.

Figure 19. Concluded.

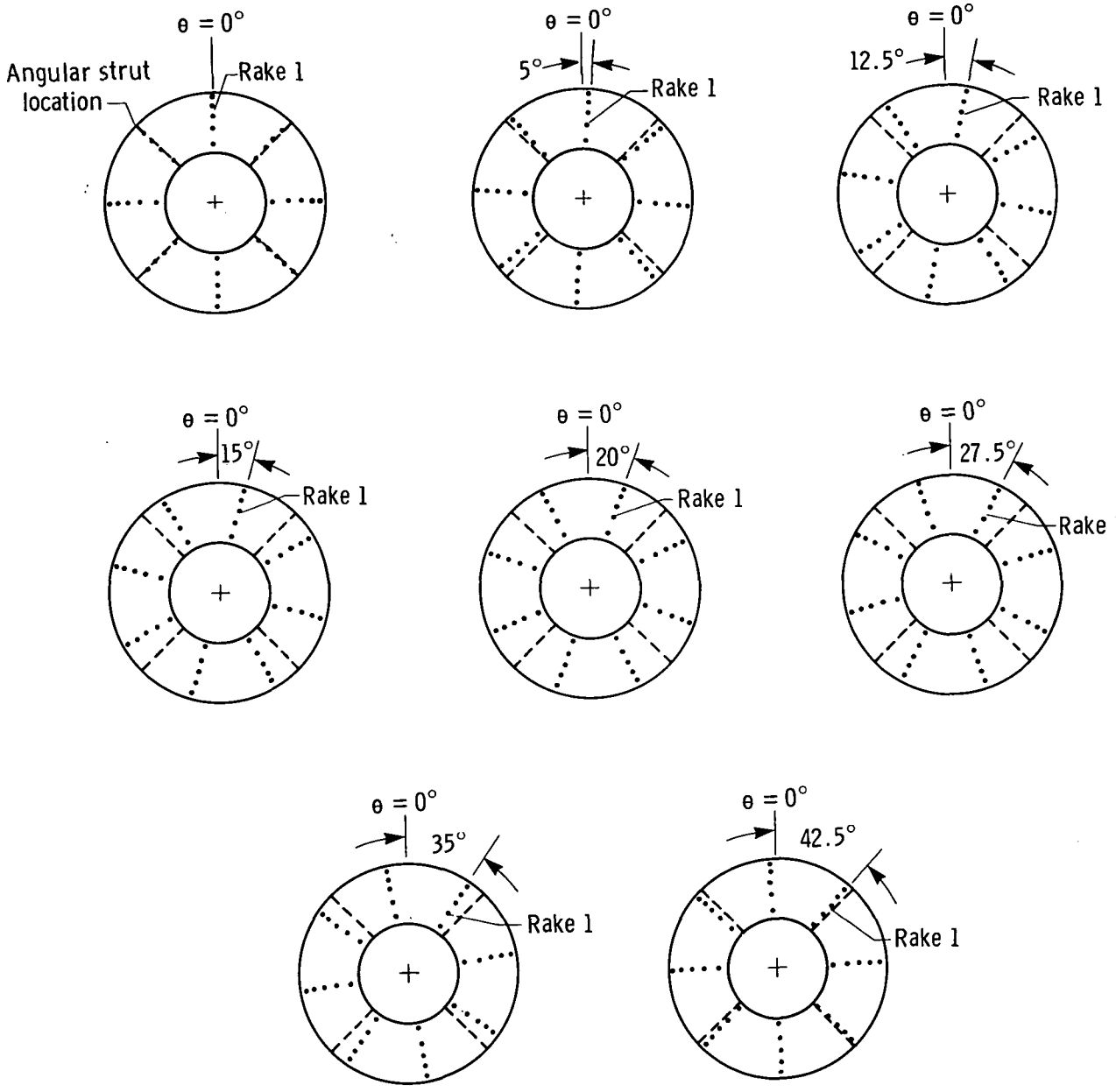

Figure 20. Rake locations with respect to strut locations for several angular locations of rake 1. Eight-rake/40-probe configuration.

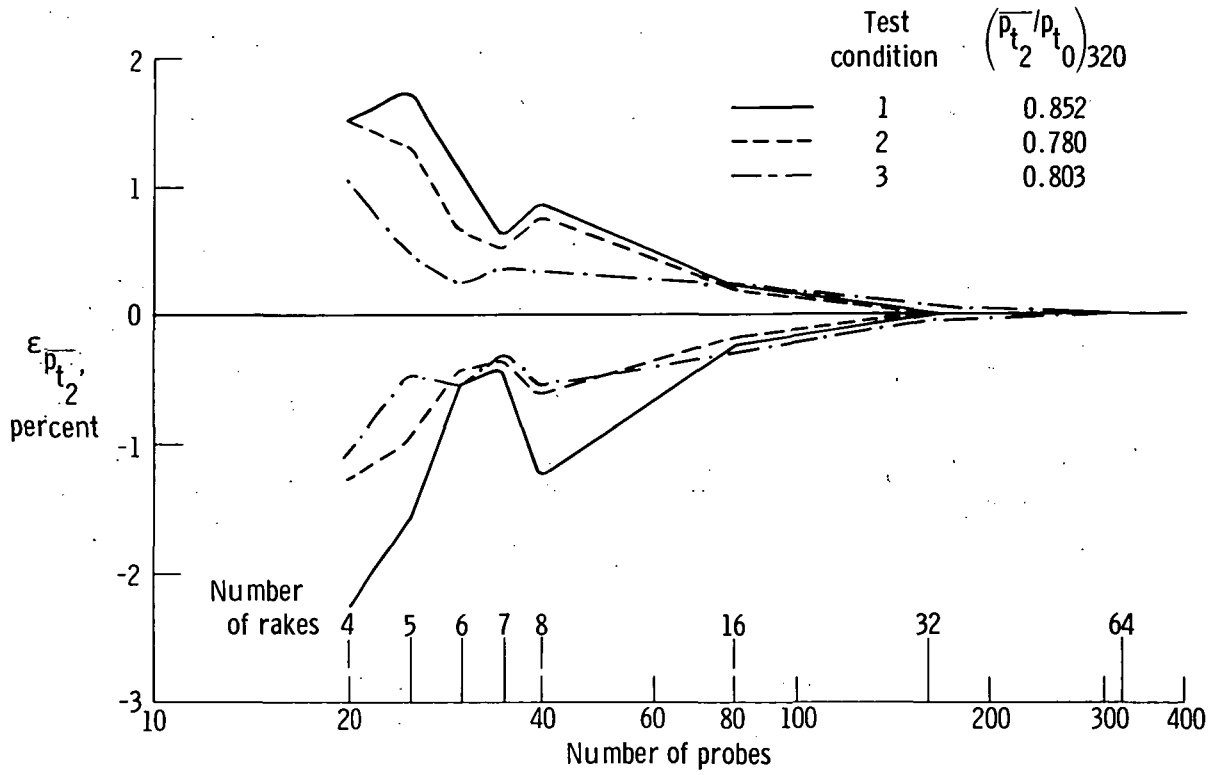

Figure 21. Variation in error of $\overline{p_{t_2}}/p_{t_0}$ *with number of rakes and probes for three test conditions.*

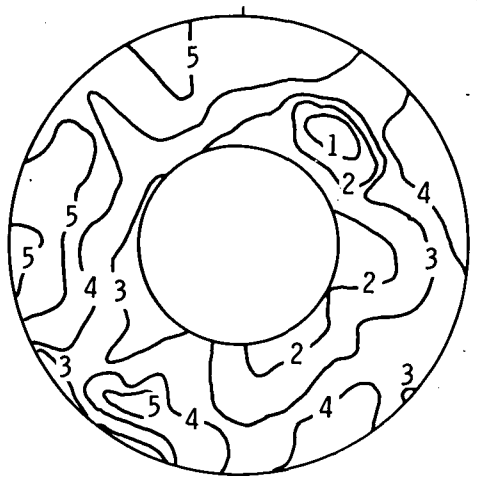

Isobar	p_{t_2}/p_{t_0}
1	0.760
2	0.795
3	0.830
4	0.865
5	0.900

(a) Sixty-four rakes, 320 probes, $\overline{p_{t_2}}/p_{t_0} = 0.852$.

$K_\theta = 0.319$, $K_r = 0.291$, $K_a = 0.609$,
IDC = 0.0804, IDT = 0.245.

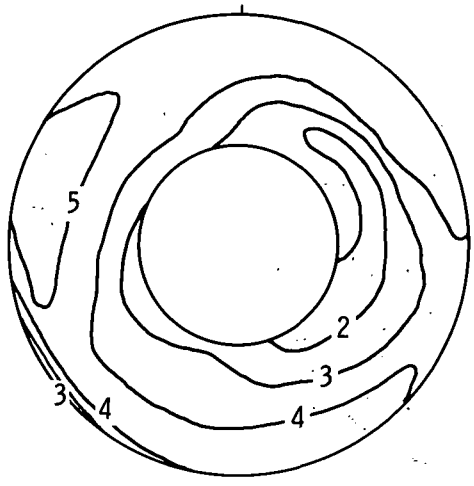

Isobar	p_{t_2}/p_{t_0}
1	0.760
2	0.795
3	0.830
4	0.865
5	0.900

(b) Eight rakes, 40 probes, $\overline{p_{t_2}}/p_{t_0} = 0.856$.

$K_\theta = 0.345$, $K_r = 0.283$, $K_a = 0.628$,
IDC = 0.0485, IDT = 0.169.

Figure 22. Pressure maps and corresponding distortion descriptors for test condition 1 using three rake configurations.

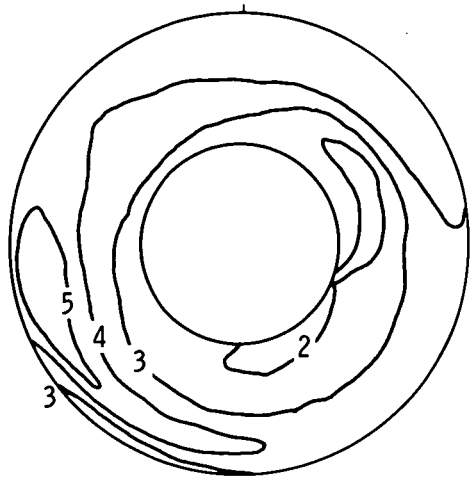

Isobar	p_{t_2}/p_{t_0}
1	0.760
2	0.795
3	0.830
4	0.865
5	0.900

(c) Seven rakes, 35 probes, $\overline{p_{t_2}}/p_{t_0} = 0.851$.

$K_\theta = 0.275$, $K_r = 0.313$, $K_a = 0.587$,
IDC = 0.0374, IDT = 0.146.

Figure 22. Concluded.

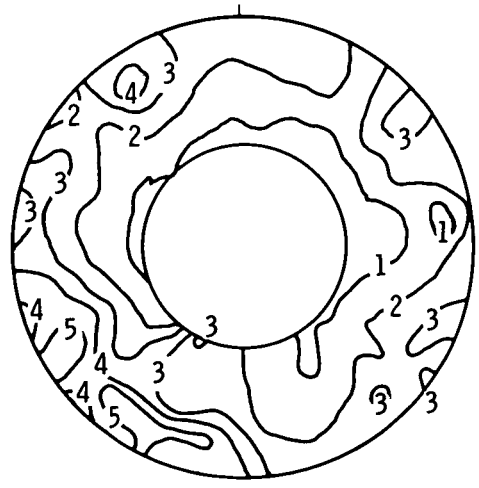

Isobar	p_{t_2}/p_{t_0}
1	0.750
2	0.773
3	0.795
4	0.818
5	0.840

(a) Sixty-four rakes, 320 probes, $\overline{p_{t_2}}/p_{t_0} = 0.780$.

$K_\theta = 0.411$, $K_r = 0.368$, $K_a = 0.779$,
IDC = 0.0551, IDT = 0.188.

Figure 23. Pressure maps and corresponding distortion descriptors for test condition 2 using three rake configurations.

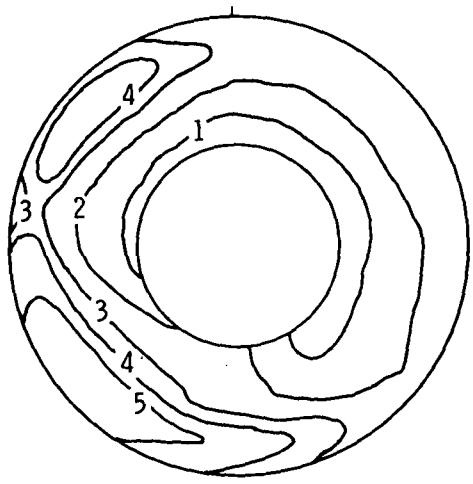

Isobar	p_{t_2}/p_{t_0}
1	0.750
2	0.773
3	0.795
4	0.818
5	0.840

(b) *Eight rakes, 40 probes,* $\overline{p_{t_2}}/p_{t_0} = 0.786$.

$K_\theta = 0.468$, $K_r = 0.474$, $K_a = 0.941$,
$IDC = 0.0392$, $IDT = 0.170$.

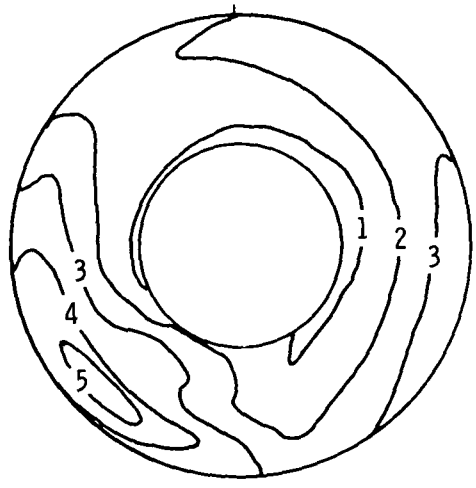

Isobar	p_{t_2}/p_{t_0}
1	0.750
2	0.773
3	0.795
4	0.818
5	0.840

(c) *Seven rakes, 35 probes,* $\overline{p_{t_2}}/p_{t_0} = 0.782$.

$K_\theta = 0.475$, $K_r = 0.355$, $K_a = 0.830$,
$IDC = 0.0345$, $IDT = 0.152$.

Figure 23. Concluded.

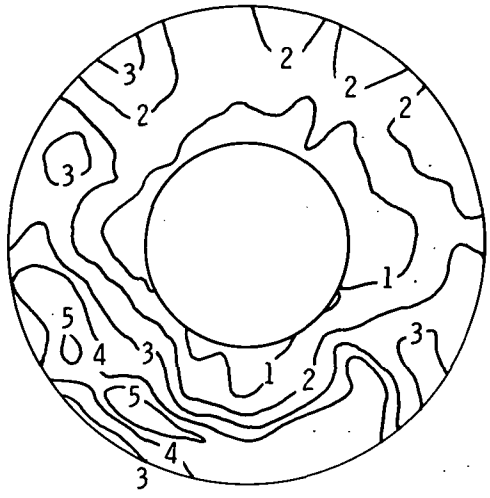

Isobar	p_{t_2}/p_{t_0}
1	0.780
2	0.798
3	0.815
4	0.833
5	0.850

(a) Sixty-four rakes, 320 probes, $\overline{p_{t_2}}/p_{t_0} = 0.802$.

$K_\theta = 0.354$, $K_r = 0.349$, $K_a = 0.703$,
IDC = 0.0321, *IDT* = 0.130.

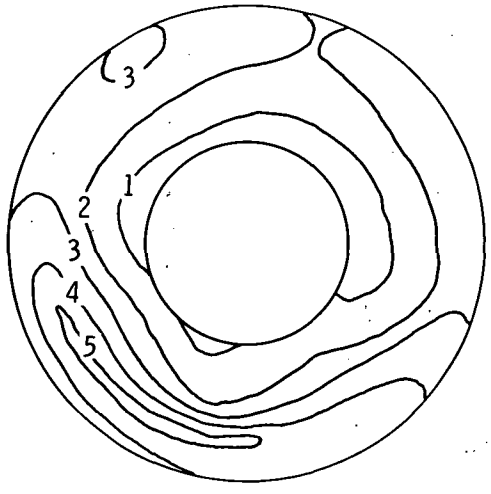

Isobar	p_{t_2}/p_{t_0}
1	0.780
2	0.798
3	0.815
4	0.833
5	0.850

(b) Eight rakes, 40 probes, $\overline{p_{t_2}}/p_{t_0} = 0.804$.

$K_\theta = 0.342$, $K_r = 0.368$, $K_a = 0.710$,
IDC = 0.0270, *IDT* = 0.101.

Figure 24. Pressure maps and corresponding distortion descriptors for test condition 3 using three rake configurations.

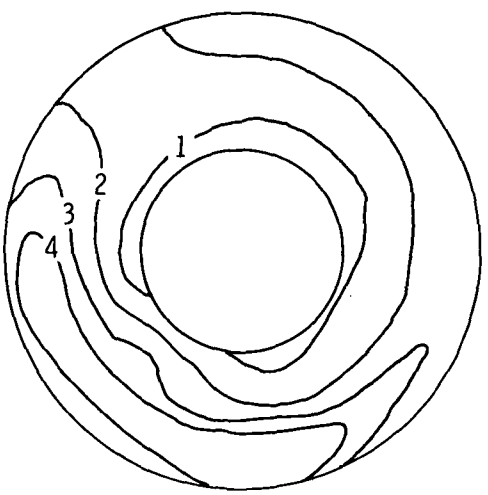

Isobar	p_{t_2}/p_{t_0}
1	0.780
2	0.798
3	0.815
4	0.833
5	0.850

(c) Seven rakes, 35 probes, $\overline{p_{t_2}/p_{t_0}} = 0.804$.

$K_\theta = 0.483$, $K_r = 0.343$, $K_a = 0.825$,
IDC = 0.0295, IDT = 0.096.

Figure 24. Concluded.

1. Report No.	2. Government Accession No.	3. Recipient's Catalog No.
NASA TM-72859		

4. Title and Subtitle	5. Report Date
EFFECT OF NUMBER OF PROBES AND THEIR ORIENTATION ON THE CALCULATION OF SEVERAL COMPRESSOR FACE DISTORTION DESCRIPTORS	May 1979
	6. Performing Organization Code

7. Author(s)	8. Performing Organization Report No.
Frederick Stoll, Jeffrey W. Tremback, and Henry H. Arnaiz	H-1070
	10. Work Unit No. 505-11-24

9. Performing Organization Name and Address	11. Contract or Grant No.
Dryden Flight Research Center P.O. Box 273 Edwards, California 93523	
	13. Type of Report and Period Covered
12. Sponsoring Agency Name and Address	Technical Memorandum
National Aeronautics and Space Administration Washington, D. C. 20546	14. Sponsoring Agency Code

15. Supplementary Notes

16. Abstract

A study was performed to determine the effects of the number and position of total pressure probes on the calculation of five compressor face distortion descriptors. This study used three sets of 320 steady state total pressure measurements that were obtained with a special rotating rake apparatus in wind tunnel tests of a mixed-compression inlet. The inlet was a one-third-scale model of the inlet on a YF-12 airplane, and it was tested in the wind tunnel at representative flight conditions at Mach numbers above 2.0.

The study showed that large errors resulted in the calculation of the distortion descriptors even with a number of probes that has been considered adequate in the past. There were errors as large as 30 and -50 percent in several distortion descriptors for a configuration consisting of eight rakes with five equal-area-weighted probes on each rake.

17. Key Words (Suggested by Author(s))	18. Distribution Statement
Compressor face distortion Compressor face pressure measurements	Unclassified - Unlimited Category: 07

19. Security Classif. (of this report)	20. Security Classif. (of this page)	21. No. of Pages	22. Price*
Unclassified	Unclassified	43	$3.75

For sale by the National Technical Information Service, Springfield, Virginia 22161

NASA-Langley, 1979

National Aeronautics and
Space Administration

Washington, D.C.
20546

Official Business
Penalty for Private Use, $300

THIRD-CLASS BULK RATE

Postage and Fees Paid
National Aeronautics and
Space Administration
NASA-451

NASA

POSTMASTER: If Undeliverable (Section 158 Postal Manual) Do Not Return